Orexin facilitates GABAergic synaptic transmission by activation of postsynaptic PKC without an increase in endocannabinoid in the rat insular cortex

Midori Chikira
Nihon University Graduate School of Dentistry
Major in Anesthesiology
(Directors: Profs. Yoshiyuki Oi and Masayuki Kobayashi,
and Assis. Prof. Kiyofumi Yamamoto)

Index

This thesis is based on the following article and additional results in terms of the effect of 2-arachidonylglycerol on unitary IPSCs (Fig. 15):

Midori Usui, Keisuke Kaneko, Yoshiyuki Oi, Masayuki Kobayashi (2019)
Orexin facilitates GABAergic IPSCs via postsynaptic OX_1 receptors coupling to the intracellular PKC signalling cascade in the rat cerebral cortex. Neuropharmacology 149:97-112.

Abstract

Orexin has multiple physiological functions including wakefulness, appetite, nicotine intake, and nociception. The cerebral cortex receives abundant orexinergic projections and expresses both orexinergic receptor 1 (OX_1R) and 2 (OX_2R). These functions are regulated by excitatory and inhibitory synaptic transmission, each of which is mediated via glutamatergic and GABAergic receptors, respectively. However, little is known about orexinergic regulation of GABA-mediated inhibitory synaptic transmission. In the cerebral cortex, there are multiple GABAergic neural subtypes, each of which has its own morphological and physiological characteristics. Therefore, identification of presynaptic GABAergic neural subtypes is critical to understand orexinergic effects on GABAergic connections. I focused on inhibitory synapses at pyramidal neurons (PNs) from fast-spiking GABAergic neurons (FSNs) in the insular cortex by a paired whole-cell patch-clamp technique, and elucidated the mechanisms of orexin-induced IPSC regulation. I found that both orexin A and orexin B enhanced unitary IPSC (uIPSC) amplitude in FSN→PN connections without changing the paired-pulse ratio or failure rate. These effects were blocked by SB-334867, an OX_1 receptor (OX_1R) antagonist, but not by TCS-OX2-29, an OX_2R antagonist. [Ala^{11}, D-Leu^{15}]-orexin B, a selective OX_2R agonist, had little effect on uIPSCs. Variance-mean analysis demonstrated an increase in quantal content without a change in release probability or the number of readily releasable pools. Laser photolysis of caged GABA revealed that orexin A enhanced GABA-mediated currents in PNs. Downstream blockade of $G_{q/11}$ protein-coupled OX_1Rs by IP_3 receptor or protein kinase C (PKC) blockers and BAPTA injection into postsynaptic PNs diminished the orexin A-induced uIPSC enhancement.

These results suggest that the orexinergic uIPSC enhancement is mediated via postsynaptic OX_1Rs, which potentiate $GABA_A$ receptors through PKC activation.

Introduction

Orexin (hypocretin) is a neuropeptide generated in a portion of the lateral and posterior hypothalamic neurons and plays multiple roles in executive physiological functions such as sleep-wake control, appetite, nicotine intake, and pain (Sakurai, 2007). There are two homologues of orexin, orexin A (hypocretin 1) and orexin B (hypocretin 2; de Lecea et al., 1998; Sakurai et al., 1998), which activate orexinergic receptors 1 (OX_1Rs) and 2 (OX_2Rs). OX_1Rs are preferentially bound by orexin A rather than orexin B, whereas OX_2Rs have almost equal preference for orexin A and orexin B (Ammoun et al., 2003; Holmqvist et al., 2001). Both OX_1Rs and OX_2Rs are coupled with $G_{q/11}$ protein and generate inositol trisphosphate (IP_3) and diacylglycerol (DAG); however, OX_2Rs are also coupled to G_i protein (Zhu et al., 2003).

The insular cortex (IC) receives multiple sensory inputs including gustation (Yamamoto et al., 1984), visceral sensation (Yasui et al., 1991), thermal sensation (Craig et al., 2000), and nociception inputs (Burkey et al., 1996; Horinuki et al., 2015; Kaneko et al., 2017; Nakamura et al., 2016, 2015). Jasmin et al. (2003) reported that IC activation enhances GABAergic neuronal activities in the locus coeruleus, and as a result, facilitates nociception by inhibiting neural activities of adrenergic projections to the spinal dorsal horn. The cerebral cortex including the IC expresses both OX_1Rs and OX_2Rs (Marcus et al., 2001) and receives orexinergic projections from the lateral hypothalamus (Nambu et al., 1999), which are considered to modulate cerebrocortical activities in combination with indirect projections via the basal forebrain, brainstem nuclei (Sutcliffe and de Lecea, 2002), and midline-intralaminar thalamic nuclei (Bayer et al., 2002; Peyron et al., 1998). Therefore, orexinergic inputs to the IC are likely to modulate nociception. Although numerous studies have demonstrated orexinergic suppression of nociception, which is mediated by the periaqueductal gray matter (Azhdari Zarmehri et al., 2011; Ho et al., 2011), posterior hypothalamic area (Bartsch et al., 2004), spinal dorsal horn (Yamamoto et al., 2003), and trigeminal spinal subnucleus caudalis (Katagiri et al., 2014), little information is available on how IC activities are regulated by orexinergic inputs.

Aracri et al. (2015) demonstrated orexin-induced modulation of EPSCs and IPSCs in the prefrontal cortex. Orexin A increases glutamate release onto fast-spiking interneurons (FSNs) and their repetitive firing frequency without changing the frequency or kinetics of miniature IPSCs (mIPSCs). However, mIPSCs involve inhibitory inputs from various cortical GABAergic interneurons including FSNs, low-threshold spike neurons, late-spiking neurons, and regular-spiking non-pyramidal neurons (Kawaguchi and Kubota, 1997; Koyanagi et al., 2010; Yamamoto et al., 2010a). Recent studies have demonstrated that these GABAergic interneurons have their own characteristic roles in regulating neural activities. For example, disinhibition of pyramidal neurons (PNs) is attributed to vasoactive-intestinal peptide-immunopositive interneurons (Pi et al., 2013), whereas somatostatin-immunopositive neurons suppress PNs with their axons that terminate on the distal dendrites of PNs (Kubota

et al., 2016). Among GABAergic interneurons, parvalbumin-immunopositive neurons, which are physiologically classified into FSNs, terminate on the somata and proximal dendrites of PNs (Kubota et al., 2016) and potently suppress PN activities by inducing large IPSCs (Koyanagi et al., 2010). Therefore, the orexinergic regulatory mechanisms depending on each type of connection are needed to be clarified to systematically determine the orexinergic regulation of cortical activity and function.

In this study, I performed paired whole-cell patch-clamp recording and analysed unitary IPSCs (uIPSCs) in FSN→PN connections to investigate how orexinergic inputs regulate FSN →PN synapses, which are the principal inhibitory regulatory circuit controlling excitatory outputs from PNs. As a result, activation of OX_1 receptors expressed on postsynaptic PNs facilitated FSN-mediated uIPSCs by increasing IP_3 and $[Ca^{2+}]_i$, which activate protein kinase C (PKC).

Materials and Methods

Ethical approval

All experiments were performed in accordance with the National Institutes of Health Guide for the Care and Use of Laboratory Animals and were approved by Institutional Animal Care and Use Committee in Nihon University. Those experiments conformed to the principles and regulations as described in the editorial by Grundy (2015). All efforts were made to minimize the number of animals used and their suffering.

Slice preparation

The data reported in this study consist of results from 89 vesicular GABA transporter (VGAT)-Venus line A transgenic rats (Nagai et al., 2002; Uematsu et al., 2008). The techniques for preparing in vitro cortical slices were similar to those previously described (Takei et al., 2017; Yamamoto and Kobayashi, 2018). Briefly, the rats of either sex, aged from 21 to 28 d, were deeply anesthetized with isoflurane (5%). After decapitation, tissue blocks including the IC were rapidly removed and stored for 3 min in ice-cold modified artificial cerebrospinal fluid (ACSF) composed of the following in mM: 230 sucrose, 2.5 KCl, 10 $MgSO_4$, 1.25 NaH_2PO_4, 26 $NaHCO_3$, 0.5 $CaCl_2$, and 10 $_D$-glucose. Coronal slices were cut at 350 μm thickness using a microslicer (Linearslicer Pro 7, Dosaka EM, Kyoto, Japan). The slices were incubated at 32 °C for 15 min in a submersion-type holding chamber that contained 50% modified ACSF and 50% normal ACSF (pH 7.35–7.40). Normal ACSF consisted of 126 NaCl, 3 KCl, 2 $MgSO_4$, 1.25 NaH_2PO_4, 26 $NaHCO_3$, 2 $CaCl_2$, and 10 $_D$-glucose in mM. Modified and normal ACSF were continuously aerated with a mixture of 95% O_2/5% CO_2. The slices were transferred to a holding chamber with normal ACSF at 32 °C for 1 h and thereafter maintained at room temperature until used for recording.

Paired whole-cell patch-clamp recordings

The slices were placed in a recording chamber that was perfused continuously with normal ACSF at a rate of 2.0 ml/min. Paired whole-cell patch-clamp recordings were obtained from Venus-positive fluorescent GABAergic interneurons identified in layer V by a fluorescence microscope equipped with Nomarski optics (40x, Olympus BX61W1, Tokyo, Japan) and an infrared-sensitive video camera (C3077-78, Hamamatsu Photonics, Hamamatsu, Japan). The distance between recorded cells was < 75 μm. Electrical signals were recorded with amplifiers (Multiclamp 700B, Molecular Devices, Sunnyvale, USA) and a digitizer (Digidata 1440A, Molecular Devices), observed on-line, and stored on a computer hard disk using Clampex (pClamp 10, Molecular Devices).

The composition of the pipette solution was as follows (in mM): 85 potassium gluconate, 70 KCl, 10 N-(2-hydroxyethyl)piperazine-N′-2-ethanesulfonic acid (HEPES; Dojin Iyaku-kako, Tokyo, Japan), 0.5 EGTA (Sigma-Aldrich), 2 $MgCl_2$, 2 magnesium adenosine triphosphate (ATP; Sigma-Aldrich; Sigma-Aldrich, St. Louis, USA), and 0.3 sodium

guanosine triphosphate (GTP; Sigma-Aldrich). The pipette solution had a pH of 7.3 and an osmolarity of 300 mOsm. The equilibrium potential of Cl^- (E_{Cl^-}) was −15 mV. In the intracellular Ca^{2+} chelation experiment, EGTA was replaced with 10mM *O,O'*-Bis(2-aminophenyl)ethyleneglycol-*N,N,N',N'*-tetraacetic acid (BAPTA; Sigma-Aldrich), and potassium gluconate was reduced to adjust the osmolarity. The liquid junction potential of the pipette solution described above was −9mV. The voltage was not corrected in the present study. Thin-wall borosilicate patch electrodes (2–5 MΩ) were pulled on a Flaming-Brown micropipette puller (P-97, Sutter Instruments, Novato, USA). Alexa Fluor 594 (Thermo Fisher Scientific, Waltham, MA, USA) was added to the internal solution in a subset of experiments to identify the neural subtypes of recorded neurons (Fig. 1A).

Recordings were obtained at 30–31 °C. The seal resistance was > 10 GΩ, and only data obtained from electrodes with access resistance of 6–20MΩ and < 20% change during recordings were included in this study. Before uIPSC recordings, the voltage responses of pre- and postsynaptic GABAergic cells were recorded by injection of depolarizing and hyperpolarizing current pulses (300 ms) to examine basic membrane properties, including input resistance, single spike kinetics, voltage-current relationship, and repetitive firing patterns and frequency. Because some cell pairs had reciprocal connections, most cells were recorded under a voltage-clamp condition (holding potential = −60 mV) during uIPSC recording. Short depolarizing voltage step pulses (2 ms, 80–120 mV) were applied to the presynaptic cells to induce action currents. The membrane currents and potentials were low-pass filtered at 5–10 kHz and digitized at 20 kHz.

Laser photostimulation using caged GABA

A laser photostimulation setup was built according to the principles reported by Deleuze and Huguenard (2006). Using this technique, I performed a selective photorelease of GABA with a caged GABA compound that uses a ruthenium complex as a photosensor. Laser photostimulation was performed using a visible wavelength laser beam (473 nm wavelength; LD laser, Olympus) directed into the port of the confocal microscopic system (FV-1000, Olympus) and the back aperture of a 60x objective (LUMPlanFl, Olympus). The position of the laser beam was adjusted with a galvanometer mirror controlled by FV-1000 software (FV-10, Olympus). The laser irradiation was cued from TTL pulses originating from the digitizer (Digidata 1440A) controlled by Clampex (Molecular Devices). To measure the laser beam power through the 60x objective, a 473-nm laser-sensitive light power meter was used (power meter console, PM100D; probe, S130VC, Thorlabs, Newton, USA). Ruthenium-bipyridine-triphenylphosphine caged GABA (Rubi-GABA; Tocris Bioscience, Ellisville, USA) was uncaged with a 104.3-μW visible wavelength pulse (19 ms).

To evoke GABA-mediated currents in a PN, laser photostimulation was applied above the PN soma, which was held at −60 mV. Stimulation interval was set at 10 s. Tetrodotoxin (1 μM, Abcam, Cambridge, UK), D-AP5 (25 μM, Abcam), and DNQX (40 μM; Abcam) were added to the ACSF to block voltage-gated Na^+ channels, NMDA receptors, and AMPA

receptors, respectively.

Alexa Fluor 647 (Thermo Fisher Scientific) was included in the intracellular solution to obtain cell morphology and determine the laser photostimulation coordinate. The E_{Cl^-} was −15 mV. I set a pipette tip filled with Rubi-GABA (2 mM) dissolved in normal ACSF several tens of μm upstream of the recorded PN for application (Pneumatic Picopomp, PV830, WPI, USA; N_2 gas, 4–5 psi). After 20 laser photostimulations, orexin A (100 nM, Sigma-Aldrich) was applied from another pipette that was set near the Rubi-GABA-containing pipette. Then, I compared the laser-evoked GABA current amplitude between the control condition and orexin A application. I confirmed that the laser-evoked GABA currents were diminished by bath application of bicuculline (10 μM, Sigma-Aldrich). Rubi-GABA is light-sensitive, and thus the laser photostimulation experiment was conducted with minimal light.

Reagents

Orexin A (100 nM) and orexin B (100 nM, Peptide Institute, Ibaraki, Japan) were applied to the perfusate except for in the laser photostimulation experiment described above. N-(2-Methyl-6-benzoxazolyl)-N″-1,5-naphthyridin-4-yl-urea (SB-334867; Nacalai tesque, Kyoto, Japan) and TCS-OX2-29 (Abcam) were used to antagonize OX_1Rs and OX_2Rs, respectively. [Ala^{11}, D-Leu^{15}]-orexin B (Wako Pure Chemical, Osaka, Japan) was used as an OX_2R-specific agonist. To inhibit PKC activity, staurosporine (Wako Pure Chemical) or chelerythrine (Sigma-Aldrich) was used. Diphenylboric acid 2-aminoethoxydiphenyl borate (2APB; Wako Pure Chemical) or xestospongin C (Wako Pure Chemical) was used as an IP_3 receptor antagonist. BAPTA (10 mM; Sigma-Aldrich) was applied to the internal solution. To confirm diffusion of BAPTA into the neurons, the current-clamp and voltage-clamp recordings were started more than 10 min after rupture of the cell membrane. Phorbol 12-myristate 13-acetate (PMA; Wako Pure Chemical), a PKC activator, was applied from the pipette set near the Rubi-GABA-containing pipette. 2-arachidonylglycerol (2-AG; Tocris), a activator of endocannabinoid, was applied to the perfusate.

Unspecified compounds were purchased from Nacalai tesque.

Data analysis

Clampfit (pClamp 10, Molecular Devices) was used for analysis of electrophysiological data. The averaged amplitude and paired-pulse ratio determined by the ratio of the peak amplitude of the second uIPSCs to that of the 1st uIPSCs were obtained from 10 to 20 consecutive sweeps. uIPSC failure was defined as a current less than 3 times the standard deviation of the baseline.

The variance-mean analysis was performed as previously described (Almado et al., 2012; Yamamoto et al., 2010b). Briefly, I obtained 20–40 uIPSCs responding to the 1st to 5th stimuli, and the mean uIPSC amplitude (M) was calculated and plotted against their varience (V). Individual plots were fitted with a quadratic equation assuming zero variance at zero amplitude. The quantal content (q) and number of release sites (N) were estimated by

expressing the equation as follows:

$$V = qM - M^2/N. \quad (1)$$

The release probability (Pr) was estimated by the equation as follows:

$$Pr = M/qN, \quad (2)$$

where M is divided by the product of the quantal content (q) and number of release sites (N).

Statistics

The values are expressed as the mean ± standard error of the mean. Differences in the mean values were compared with the paired *t*-test or Student's *t*-test, and the Wilcoxon signed-rank test was used for a comparison of failure rate, the distribution of which could not be fitted with a normal distribution. Differences with a probability (P) less than 0.05 were considered significant.

Results

The present study focused on GABAergic synaptic transmission from FSN → PN connections in layer V of the IC. To discriminate glutamatergic and GABAergic neurons, I used VGAT-Venus line A transgenic rats in which GABAergic neurons are marked with a green fluorescent protein, Venus (Fig. 1A). FSNs were identified as Venus-positive and characteristic firing properties neurons: high firing rate (typically > 100 Hz) without spike adaptation, short spike duration, and large and short afterhyperpolarization (AHP; Galarreta and Hestrin, 2002; Kawaguchi and Kubota, 1997; Koyanagi et al., 2010, 2014; Yamamoto et al., 2010a; Yamamoto and Kobayashi, 2018, Fig. 1B). On the other hand, PNs were Venus-negative and characterized by a pyramidalshaped soma with a vertical apical dendrite. Short depolarizing pulse injection (Fig. 1C, top) induced action current in an FSN (Fig. 1C, middle), which elicited uIPSCs in the simultaneously recorded PN (Fig. 1C, bottom).

Orexin A and orexin B enhance uIPSCs in FSN→PN connections

The effects of orexin homologues, orexin A and orexin B, on uIPSCs in FSN→PN connections were examined (Figs. 2 and 3). Bath application of 100 nM orexin A enhanced uIPSCs (Fig. 2A), and this facilitative effect was washable (Fig. 2A, B). In 28 FSN→PN connections, orexin A (100 nM) significantly increased the amplitude of uIPSCs from 81.9 ± 15.3 pA to 102.8 ± 21.2 pA (43.8%; $P < 0.05$; paired *t*-test; Fig. 2D).

In addition to the first uIPSCs, orexin A also enhanced subsequent uIPSCs (Fig. 2C). Although the 1st uIPSCs tended to be most sensitive to orexin A, the amplitude of the 1st to 5th uIPSCs showed a significant increase by orexin A (Fig. 2C; $P < 0.05$; paired *t*-test). This facilitation was not associated with a change in the paired-pulse ratio (2nd uIPSC amplitude/1st uIPSC amplitude) induced by orexin A (0.71 ± 0.04 in control and 0.72 ± 0.04 during orexin A application, n = 28; P = 0.73; paired *t*-test; Fig. 2D). Moreover, no significant change was observed in failure rate after orexin A application (12.1 ± 4.2% in control and 10.4 ± 3.7% during orexin A application, n = 28; P = 0.72; Wilcoxon signed-rank test; Fig. 2D).

Similar to orexin A, application of 100 nM orexin B enhanced uIPSCs (Fig. 3A), and the effect was washable (Fig. 3A, B). In 19 FSN→PN connections, orexin B (100 nM) significantly increased the amplitude of uIPSCs from 50.2 ± 9.3 pA to 62.1 ± 12.3 pA (33.3%; $P < 0.05$; paired *t*-test; Fig. 3D) with little effect on the subsequent uIPSC amplitude (P = 0.44; paired *t*-test; Fig. 3C). The paired-pulse ratio (0.78 ± 0.07 in control and 0.65 ± 0.03 during orexin B application, n = 19; P = 0.09; paired *t*-test) and failure rate (13.7 ± 4.7% in control and 7.9 ± 2.6% during orexin B application, n = 19; P = 0.86; Wilcoxon signed-rank test) were also insensitive to orexin B (Fig. 3D).

OX_2Rs play a minor role in the orexin A/B-induced facilitation of uIPSCs

Although both OX_1Rs and OX_2Rs are activated by orexin A and orexin B, their binding

preferences are different: OX_1Rs have a 50-times higher preference for orexin A than orexin B, whereas OX_2Rs have almost equal preference to orexin A and orexin B (Ammoun et al., 2003; Holmqvist et al., 2001). To examine which orexinergic receptor contributes to the enhancement of uIPSCs, I first applied the selective OX_2R agonist, [Ala^{11}, D-Leu^{15}]-orexin B.

The amplitude of uIPSCs in FSN→PN connections was insensitive to bath application of 1 μM [Ala^{11}, D-Leu^{15}]-orexin B: 103.7 ± 48.7 pA in control and 102.1 ± 47.5 pA during [Ala^{11}, D-Leu^{15}]-orexin B application (n = 9; P = 0.74, paired *t*-test; Fig. 4A–C). Furthermore, [Ala^{11}, D-Leu^{15}]-orexin B had little effect on the paired-pulse ratio (0.69 ± 0.06 in control and 0.63 ± 0.07 during [Ala^{11}, D-Leu^{15}]-orexin B application, n = 9; P = 0.21, paired *t*-test) and failure rate (8.9 ± 6.5% in control and 16.7 ± 9.9% during [Ala^{11}, D-Leu^{15}]-orexin B application, n = 9; P = 0.13, Wilcoxon signed-rank test; Fig. 4D).

Application of TCS-OX2-29, an OX_2R antagonist, supported the finding that the orexin A/B-induced uIPSC enhancement is less mediated via OX_2Rs. Orexin A (100 nM) application in combination with TCS-OX2-29 enhanced uIPSCs (121.0 ± 37.0 pA to 138.0 ± 38.0 pA, n = 8; P < 0.05, paired *t*-test; Fig. 5), whereas the paired-pulse ratio (0.75 ± 0.08 to 0.68 ± 0.03, n = 8; P = 0.47, paired *t*-test) and failure rate (7.5 ± 4.9% to 3.8 ± 3.8%, n = 8; P = 0.56, Wilcoxon signed-rank test) were insensitive to orexin A under TCS-OX2-29 application (Fig. 5D).

Similarly, 100 nM orexin B increased uIPSC amplitude under TCS-OX2-29 application: 62.9 ± 19.8 pA during TCS-OX2-29 application and 73.8 ± 23.5 pA during orexin B application with TCS-OX2-29 (n = 11; P < 0.05, paired *t*-test; Fig. 6). The paired-pulse ratio (0.67 ± 0.17 during TCS-OX2-29 application and 0.59 ± 0.11 during orexin B application with TCS-OX2-29, n = 11; P = 0.60, paired *t*-test) and failure rate (21.8 ± 8.3% during TCS-OX2-29 application and 16.4 ± 5.1% during orexin B application with TCS-OX2-29, n = 11; P = 0.38, Wilcoxon signed-rank test) were insensitive to orexin B under TCS-OX2-29 application (Fig. 6D).

These results indicate that the OX_2R antagonist had no significant effect on the orexin A/B-induced enhancement of uIPSCs, and, therefore, OX_2Rs are unlikely to be involved in the orexinergic enhancement of uIPSCs in FSN→PN connections.

OX_1 receptors play a crucial role in the orexin A/B-induced facilitation of uIPSCs

The findings using the OX_2R agonist and application of orexin A or orexin B with the OX_2R antagonist described above led to the hypothesis that orexinergic enhancement of uIPSCs in FSN→PN connections is mediated via OX_1Rs. To test this, I next examined the effect of preceding application of SB-334867, a selective OX_1R antagonist, on the orexin A-induced enhancement of uIPSCs in FSN→PN connections. In the present study, I did not examine the effect of a selective OX_1R agonist because there is none commercially available so far.

Under application of 10 μM SB-334867, orexin A (100 nM) had little effect on uIPSCs (96.1 ± 20.5 pA to 90.5 ± 18.0 pA, n = 7; P = 0.28, paired *t*-test; Fig. 7). In addition, the

paired-pulse ratio (0.67 ± 0.09 to 0.69 ± 0.06, n = 7; P = 0.86, paired *t*-test) and failure rate (4.3 ± 3.0% to 1.4 ± 1.4%, n = 7; P = 0.16, Wilcoxon signed-rank test) were also insensitive to orexin A (Fig. 7D). In agreement with the effects of orexin A and SB-334867 application, orexin B (100 nM) also had little effect on the amplitude (78.8 ± 25.5 pA to 75.1 ± 19.0 pA, n = 10; P = 0.63, paired *t*-test), paired-pulse ratio (0.62 ± 0.06% to 0.61 ± 0.07%, n = 10; P = 0.90, paired *t*-test), and failure rate (17.0 ± 7.8 to 15.0 ± 7.2, n = 10; P = 0.41, Wilcoxon signed-rank test) under application of SB-334867 in FSN→PN connections (Fig. 8).

These results suggest that OX_1Rs primarily mediate the orexinergic enhancement of uIPSCs in FSN→PN connections.

Variance-mean analysis to examine the targeted site of orexin A

An enhancement of uIPSCs by orexin A and orexin B without a change in paired-pulse ratio or failure rate suggests that this orexinergic effect is mediated by a postsynaptic mechanism, reflected by a larger quantal size (q) rather than larger release probability (Pr) or number of release sites (N). To examine this possibility, I employed variancemean analysis and evaluated three parameters of synaptic function (q, Pr, and N) using uIPSCs recorded from FSN→PN connections in the control condition and during application of orexin A (Fig. 9). To alter the release probability, 5 train pulses at 20 Hz were applied to presynaptic FSNs (Fig. 9A).

The variance calculated from 30 traces in the control condition and during application of orexin A was plotted against the averaged amplitude of the respective uIPSCs. The plots were fitted with a seconddegree polynomial equation (Fig. 9B), and I obtained q, Pr, and N (see the Materials and Methods).

As a result, a larger q was detected during orexin A application (19.7 ± 2.9 pA, n = 18) than during control (13.9 ± 3.4 pA, n = 18; P < 0.05; paired *t*-test; Fig. 9C). On the other hands, the Pr was comparable between control and orexin A application: 38.2 ± 5.2% and 42.7 ± 13.1% (n = 18; P = 0.76, paired *t*-test; Fig. 9C). Similar to Pr, N was comparable between control (16.7 ± 3.7, n = 18) and orexin A application (12.5 ± 2.6, n = 18; P = 0.21, paired *t*-test; Fig. 9C). These results suggest that the orexin A-induced enhancement of uIPSCs is mediated by a postsynaptic mechanism, an increase in q, in FSN→PN connections.

Orexin A enhances postsynaptic GABAergic currents

The profile of the orexinergic effects on uIPSCs, i.e., uIPSC enhancement without a change in paired-pulse ratio or failure rate, and the results obtained from the variance-mean analysis strongly suggest that postsynaptic OX_1Rs enhance uIPSCs as described above. To confirm this hypothesis, I further examined the effect of orexin A application on GABA-mediated inward currents recorded from PNs (Fig. 10). I used a laser photostimulation method to apply GABA instantaneously because puff application of GABA often induces rundown of GABA-mediated currents. Rubi-GABA (2 mM) was continuously applied from the patch pipette located upstream of the recorded PN (Fig. 10A, B). GABA-mediated currents were

induced by laser photostimulation nearby the recorded PN. A pipette filled with orexin A (100 nM) was also set upstream of the PN, and orexin A was ejected by continuous air pressure application to the pipette as needed (Fig. 10A).

GABAergic currents were consistently evoked by laser photostimulation (Fig. 10C). Little rundown of the currents was observed during photostimulation at 10s intervals (Fig. 10D). Application of orexin A effectively enhanced the GABA-mediated currents as shown in Fig. 10C, D. The amplitude of GABAergic currents was significantly enhanced by orexin A application from 108.2 ± 39.0 pA to 131.6 ± 42.1 pA (n = 9; P < 0.01, paired *t*-test; Fig. 10E). These results support the hypothesis that the orexin-induced enhancement of uIPSCs is mediated through postsynaptic orexinergic receptors.

IP_3 and PKC contribute to the orexinergic enhancement of uIPSCs

Both OX_1Rs and OX_2Rs are coupled to $G_{q/11}$ protein and generate IP_3 and DAG, although OX_2Rs are also coupled to G_i protein (Zhu et al., 2003). If the orexin A/B-induced enhancement of uIPSCs is mediated by OX_1Rs, blockade of a second messenger downstream of $G_{q/11}$, IP_3 and inhibition of PKC should diminish the uIPSC enhancement. Thus, I examined the effect of orexin A on uIPSC amplitude in combination with a membrane-permeable IP_3 receptor antagonist, 2APB or xestospongin C, and with a PKC inhibitor, staurosporine or chelerythrine.

Orexin A (100 nM) application under preapplication of 2APB (15 μM) had little effect on uIPSC amplitude: 67.8 ± 13.8 pA with 2APB preapplication and 60.0 ± 15.7 pA with orexin A and 2APB (n = 13; P = 0.48, paired *t*-test; Fig. 11). In addition, the paired-pulse ratio (0.67 ± 0.05 with 2APB preapplication and 0.68 ± 0.03 with orexin A and 2APB, n = 13; P = 0.92, paired *t*-test) and failure rate (2.3 ± 1.2% with 2APB preapplication and 3.8 ± 1.8% with orexin A and 2APB, n = 13; P = 0.56, Wilcoxon signed-rank test) were also not changed by co-application of orexin A with 2APB (Fig. 11D).

Similarly, preapplication of xestospongin C (1 μM) inhibited the orexin A-induced uIPSC enhancement. uIPSC amplitude under application of xestospongin C (25.1 ± 7.6 pA) was not changed by orexin A (100 nM; 25.5 ± 8.0 pA, n = 13; P = 0.81, paired *t*-test; Fig. 11E–H). The paired-pulse ratio (0.83 ± 0.11 with xestospongin C preapplication and 0.73 ± 0.06 with orexin A and xestospongin C, n = 13; P = 0.28, paired *t*-test) and failure rate (13.8 ± 6.7% with xestospongin C preapplication and 20.0 ± 7.4% with orexin A and xestospongin C, n = 13; P = 0.28, Wilcoxon signed-rank test) were also not changed by co-application of orexin A with xestospongin C (Fig. 11H). These results suggest that the orexin A-induced enhancement of uIPSCs is mediated by an increase in IP_3.

In terms of PKC blockade, preapplication of staurosporine (1 μM) also inhibited the uIPSC enhancement by orexin A (100 nM): 98.2 ± 40.2 pA with staurosporine preapplication and

105.8 ± 45.2 pA with orexin A and staurosporine (n = 11; P = 0.30, paired *t*-test; Fig. 12). In addition, orexin A with staurosporine did not change the paired-pulse ratio (0.74 ± 0.04 with staurosporine preapplication and 0.66 ± 0.06 with orexin A and staurosporine, n = 11; P = 0.27,

paired *t*-test) or failure rate (20.0 ± 9.7% with staurosporine preapplication and 19.0 ± 7.2% with orexin A and staurosporine, n = 11; P = 0.89, Wilcoxon signed-rank test) as shown in Fig. 12D.

Orexin A (100 nM) application under preapplication of chelerythrine (1 μM) had little effect on uIPSC amplitude: 114.5 ± 30.8 pA with chelerythrine preapplication and 95.6 ± 25.5 pA with orexin A and chelerythrine (n = 8; P = 0.10, paired *t*-test; Fig. 12E–H). In addition, the paired-pulse ratio (0.67 ± 0.06 with chelerythrine preapplication and 0.71 ± 0.06 with orexin A and chelerythrine, n = 8; P = 0.55, paired *t*-test) and failure rate (2.5 ± 1.6% with chelerythrine preapplication and 1.3 ± 1.3% with orexin A and chelerythrine, n = 8; P = 0.32, Wilcoxon signed-rank test) were also not changed by co-application of orexin A with chelerythrine (Fig. 12H). These results suggest that PKC contributes to the orexin A-induced enhancement of uIPSCs.

Postsynaptic Ca^{2+} chelation blocks the orexinergic enhancement of uIPSCs

An increase in IP_3 induces an increase in $[Ca^{2+}]_i$ by releasing stored Ca^{2+} from the endoplasmic reticulum, which in turn mediates PKC activation. Considering that the postsynaptic OX_1R likely mediates the orexin A-induced uIPSC enhancement, Ca^{2+} chelation of postsynaptic PNs should suppress the orexin A-induced enhancement of uIPSCs. Thus, I finally examined the effect of Ca^{2+} chelation by adding BAPTA to the solution in the pipette patched onto postsynaptic PNs.

I performed whole-cell patch-clamp recordings from FSNs and PNs using an intracellular patch solution without and with BAPTA (10 mM), respectively. To confirm that BAPTA effectively chelated Ca^{2+} in PNs, kinetics of the action potential and AHP, a portion of which are regulated by Ca^{2+}-dependent K^+ currents (Sah, 1996; Sun et al., 2003), were examined and compared to those recorded with an intracellular pipette solution without BAPTA. I applied long (300 ms) depolarizing current pulses to induce repetitive action potentials (8 spikes/300 ms) and quantified the half-duration of the 8th action potential to avoid the effect of a transient K^+ current (A-current; Fig. 13A). Repetitive spike firing induced a medium-duration AHP just after current termination, and the peak amplitude of the mediumduration AHP was estimated (Fig. 13A).

Intracellular application of 10 mM BAPTA significantly increased the half-duration of action potentials (6.8 ± 0.5 ms, n = 31) in comparison to the solution lacking BAPTA (4.6 ± 0.3 ms, n = 25; P < 0.001; Student's *t*-test; Fig. 13B–D). In addition, BAPTA reduced the peak amplitude of the medium-duration AHP amplitude (2.1 ± 0.3 mV, n = 31) in comparison to the solution lacking BAPTA (4.9 ± 0.4 mV, n = 25; P < 0.001, Student's *t*-test; Fig. 13B–D). These results indicate that BAPTA certainly chelated intracellular Ca^{2+} using my injection protocol.

After confirming the effect of BAPTA on the spike kinetics of PNs, I recorded uIPSCs. Under the BAPTA-injected condition, PNs showed little effect of orexin A (100 nM) on uIPSC amplitude (28.7 ± 6.3 pA in control and 29.1 ± 7.4 pA during orexin A application; n =

10; P = 0.89, paired *t*-test; Fig. 13E–G). The paired-pulse ratio was also unaffected by orexin A (0.76 ± 0.09 in control and 0.60 ± 0.07 during orexin A application, n = 10; P = 0.09, paired *t*-test, Fig. 13G). Similarly, the failure rate was not changed by orexin A (2.5 ± 2.5% in control and 3.3 ± 2.6% during orexin A application, n = 10; P = 0.32, Wilcoxon signed-rank test; Fig. 13G). These results support my hypothesis that orexin A facilitates uIPSCs via postsynaptic OX_1Rs that generate IP_3, increase Ca^{2+}, and activate PKC.

PKC-dependent enhancement of GABAergic currents by orexin A

To confirm the involvement of IP_3 and PKC pathway, the effects of xestospongin C and chelerythrine, which inhibit IP_3 receptors and PKC, respectively, on the enhancement of GABA-mediated currents by orexin A were examined using the same recording setup shown in Fig. 10A. In addition, I examined effects of PMA, a PKC activator, on GABAmediated currents.

Under bath application of xestospongin C (1 μM), GABA-mediated currents recorded from PNs (61.8 ± 20.0 pA) were not changed by 100 nM orexin A (61.2 ± 19.6 pA, n = 9; P = 0.80, paired *t*-test; Fig. 14A,D). Similarly, under bath application of chelerythrine (1 μM), GABA-mediated currents recorded from PNs (60.9 ± 13.3 pA) were not changed by 100 nM orexin A (60.5 ± 10.7 pA, n = 13; P = 0.93, paired *t*-test; Fig. 14B,D). On the other hand, 2 μM PMA application from the patch pipette set upstream of the PN enhanced GABA-mediated currents from 83.7 ± 33.7 pA to 127.2 ± 37.1 pA (n = 10; P < 0.05, paired *t*-test; Fig. 14C, D).

These results support the hypothesis that orexin A enhances IPSCs via a postsynaptic mechanism involving IP_3 receptor and PKC activation.

Endocannabinoids do not enhance uIPSCs in FSN→PN connections

Ho et al (2011) demonstrated that activation of OX_1R triggers the synthesis of the endocannabinoid (eCB) which depresses the release of glutamate and GABA in the brain. Therefore, there is a possibility that the increase of eCB signaling contributed to the overall effect of OX_1R on GABA-IPSCs. To test this, I examined the effect of 2-arachidonylglycerol (2-AG; 1 μM), a activator of endocannabinoid, on uIPSCs in FSN→PN connections. The amplitude of uIPSCs in FSN→PN connections was insensitive to bath application of 1 μM 2-AG: 79.6 ±34.0 pA in control and 80.8 ±32.5 pA during 2-AG application (n = 11; P = 0.76, paired *t*-test; Fig. 15 A–C). Furthermore, 2-AG had little effect on the paired-pulse ratio (0.85 ± 0.14 in control and 0.69 ± 0.08 during 2-AG application, n = 11; P = 0.19, paired *t*-test), and failure rate (11.8 ± 5.0% in control and 9.1 ± 4.8% during 2-AG application, n = 11; P = 0.45, Wilcoxon signed-rank test; Fig. 15D).

These result indicate that the orexin A-induced enhancement of uIPSCs is unlikely to be involved in the endocannabinoid signaling in FSN→PN connections.

Discussion

Which synaptic site, presynaptic or postsynaptic, is targeted by orexin?

The cerebral cortex expresses both OX_1Rs and OX_2Rs and receives abundant orexinergic fibres (Marcus et al., 2001; Peyron et al., 1998). Mechanisms of orexinergic regulation of EPSCs have been studied in the prefrontal cortex. Lambe et al. (2007) reported that presynaptic hypocretin receptor type 2 depolarizes the membrane potential, which increases cation influx and glutamate release. Similarly, hypocretin increases spontaneous and miniature EPSCs recorded from FSNs without changing their amplitude, suggesting orexinergic facilitation of glutamate release onto FSNs (Aracri et al., 2015).

On the other hand, little information has been available on how orexin regulates IPSCs in the cerebral cortex except for the study by Aracri et al. (2015), who reported that hypocretin increases spontaneous IPSC frequency and amplitude in PNs but that miniature IPSCs are insensitive to hypocretin. These findings suggest that hypocretin facilitates spike firing of inhibitory neurons projecting to PNs but has little effect on GABA release. Other than the effects in the cerebral cortex, orexinergic effects on IPSCs in other brain region have been reported in several studies. Ventrolateral periaqueductal gray neurons exhibit a postsynaptic OX_1R-dependent mechanism of IPSC modulation, in which activated OX_1Rs lead to the generation of endocannabinoid and induce retrograde inhibition of GABA release (Ho et al., 2011). On the other hand, orexin A induces presynaptic suppression of GABA release in cardiac vagal neurons (Dergacheva et al., 2012). Consistent with their study, hypocretin increases the frequency of spontaneous and miniature IPSCs in neurons of the dorsal motor nucleus of the vagus nerve, suggesting a presynaptic action of orexin (Davis et al., 2003). Thus, whether orexin changes GABAergic synaptic transmission and which synaptic site, presynaptic or postsynaptic, is targeted by orexin to modulate GABAergic synaptic transmission have been controversial.

The present studies strongly suggest postsynaptic mechanisms of the orexin-induced potentiation of IPSCs in FSN→PN connections. This finding contradicts the little change in mIPSCs induced by hypocretin in the prefrontal PNs (Aracri et al., 2015). A possible reason for this discrepancy is that mIPSCs involve GABAergic inputs from not only FSNs but also various other GABAergic neurons: if IPSCs in non-FSN→PN connections are insensitive to orexin, the enhancement of mIPSCs from FSNs to PNs may be masked. Furthermore, orexinergic modulation profiles may also be different among the cortical areas.

Downstream signalling of OX_1Rs

Even though no information is available on the effects of an OX_1R selective agonist, my pharmacological experiments strongly suggest that the orexinergic facilitation of GABA-mediated inhibitory synaptic transmission is mediated by postsynaptic OX_1Rs, which are coupled with $G_{q/11}$ (Zhu et al., 2003). The effector of $G_{q/11}$ is phospholipase C, which cleaves the phospholipid phosphatidylinositol 4,5-bisphosphate (PIP_2) into IP_3 and DAG. IP_3

acts on IP_3 receptors expressed in the endoplasmic reticulum membrane and releases Ca^{2+} stored in the endoplasmic reticulum through these receptors (Berridge, 1998). The released Ca^{2+} collaborates with DAG in PKC. Therefore, orexin A and orexin B can be reasonably postulated to enhance $GABA_A$ receptormediated IPSCs by activating this intracellular signalling cascade and downstream factors of OX_1Rs.

My findings support this hypothesis. First, the PKC inhibitor staurosporine or chelerythrine effectively diminished the orexin A-induced enhancement of uIPSCs and GABA-mediated currents. Second, orexin A had little effect on uIPSCs and GABA-mediated currents under application of the membrane-permeable IP_3 receptor antagonist, 2APB or xestospongin C. Third, the orexin A-induced enhancement of uIPSCs was not observed with intracellular administration of the potent Ca^{2+} chelator, BAPTA. Fourth, the PKC activator PMA enhanced GABAmediated currents. Taken together with the discussion described in the previous section, these observations suggest that orexin A/B may facilitate uIPSCs in FSN→PN connections by phosphorylating $GABA_A$ receptors expressed in postsynaptic PNs with PKC.

Notably, $GABA_A$ receptor activity is regulated by phosphorylation of several protein kinases including PKA and PKC (Kittler and Moss, 2003). The results of PKA activation are inconsistent: e.g., PKA decreases GABA-mediated currents in hippocampal PNs (Poisbeau et al., 1999) but increases them in granule cells in the olfactory bulb (Nusser et al., 1999). On the other hand, Brandon et al. (2002) reported that PKC activation induces a more consistent effect on $GABA_A$ receptors, i.e., suppression of $GABA_A$ receptor function. In cortical neurons, PKC phosphorylates the β3 subunit of $GABA_A$ receptors, which suppresses $GABA_A$ receptor-mediated currents (Brandon et al., 2000). The present findings contradict these reports. Interestingly Poisbeau et al. (1999) reported that hippocampal CA1 PNs and dentate gyrus granule cells exhibit discrepant effects of PKC activation on miniature IPSCs: no effect in the former but enhancement in the latter. The present results are in the same line as those for the dentate gyrus granule cells, potentially due to a difference in $GABA_A$ subunit expression as Brandon et al. (2002) suggested.

The mitogen-activated protein kinase (MAPK) pathway, including Raf, MEK, and extracellular signal-regulated kinase (ERK), is known to be activated by PKC isotypes including the Ca^{2+}-dependent conventional PKC (Schönwasser et al., 1998). My previous study demonstrated that gustatory stimulation induces phosphorylation of ERK1/2 in PNs of the IC, though I did not examine the relationship between PKC and ERK1/2 phosphorylation (Kobayashi et al., 2010). Indeed, PKC-dependent phosphorylation of ERK1/2 is reported in cerebrocortical neurons (Lai et al., 2016). These findings imply another possibility that kinases in the MAPK pathway downstream of PKC might regulate $GABA_A$ function.

Functional implications

Orexin-dependent suppression of nociception has been reported in acute and chronic pain models: e.g., intrathecal application of orexin A induces an analgesic effect in the formalin test and hot-plate test (Bingham et al., 2001; Yamamoto et al., 2002), and in neuropathic

models, orexin A attenuates incision-induced allodynia (Cheng et al., 2003) and diabetic neuropathy (Kajiyama et al., 2005). The orexin A-induced suppression of nociception is diminished by an OX_1R antagonist (Bingham et al., 2001; Cheng et al., 2003; Kajiyama et al., 2005; Yamamoto et al., 2003). Focal application of orexinergic agonists and antagonist reveals several key brain regions that play a critical role in the suppression of nociception, i.e., the posterior hypothalamic area (Bartsch et al., 2004), periaqueductal gray matter (Azhdari Zarmehri et al., 2011; Ho et al., 2011), spinal dorsal horn (Yamamoto et al., 2003), and trigeminal subnucleus caudalis (Bahaaddini et al., 2016; Katagiri et al., 2014). Inutsuka et al. (2016) clearly demonstrated that selective ablation of orexinergic neurons in the lateral hypothalamic area enhances pain-related behaviours and that orexinergic neurons are activated by nociceptive inputs.

However, little information has been available on the orexinergic effects on cerebrocortical neural activities. The IC plays a critical role in nociceptive information processing including tooth pulp sensation (Nakamura et al., 2016, 2015) and is likely to enhance nociception via regulation of activities of the locus coeruleus (Jasmin et al., 2003). Therefore, the present results contribute to the understanding of cortical mechanisms that control nociceptive information processing, and suggest that orexinergic activation targeting the IC could be used for chronic pain treatment.

In addition to nociception, the dorsal IC processes gustatory and visceral information (Yamamoto et al., 1984; Yasui et al., 1991). Taking into account of orexinergic inputs from the lateral hypothalamus, a part of the feeding centre (Sakurai et al., 1998), the uIPSC enhancement in PNs may contribute to suppression of gustation and visceral sensation, which is possibly involved in feeding behaviours.

Notably, the IC has also been considered to play a role in addiction. IC damage in human smokers induces spontaneous cessation of smoking (Naqvi et al., 2007). Interestingly, the blockade of OX_1Rs in the dorsal part of the IC (Hollander et al., 2008), a part of which overlaps with the gustatory (Yamamoto et al., 1984) and/or nociceptive areas (Nakamura et al., 2016, 2015), decreases nicotine self-administration. In addition, intraperitoneal injection of SB-334867, an OX_1R antagonist, attenuates cue-induced reinstatement of nicotine-seeking, and PKC-dependent phosphorylation of p38 MAPK in the nucleus accumbens is involved in relapse to nicotine-seeking (Plaza-Zabala et al., 2013). Therefore, orexinergic inputs to the IC and other brain regions such as the nucleus accumbens are likely necessary to maintain tobacco addiction in humans (Kenny, 2011). The present finding of a postsynaptic OX_1R-dependent enhancement of FSN→PN synaptic transmission could be involved in tobacco addiction.

Conclusions

The present study demonstrated that both orexin A and orexin B enhanced uIPSCs in FSN →PN connections, and this orexin-induced potentiation of uIPSCs was effectively blocked by preapplication of SB-334867 but not TCS-OX2-29, suggesting that the orexin A/B-induced

enhancement of uIPSCs is principally mediated by OX_1Rs but not OX_2Rs. This hypothesis was supported by the small effect of a selective OX_2R agonist, [Ala^{11}, D-Leu^{15}]-orexin B, on uIPSCs. Variance-mean analysis and Rubi-GABA experiments strongly suggested that the orexin A-induced enhancement of uIPSCs is mediated by potentiation of postsynaptic $GABA_A$ receptors. Furthermore, I elucidated the mechanism of the orexinergic facilitation of uIPSCs that elevation of intracellular Ca^{2+} via IP^3 receptor activation and PKC activation were necessary to enhance $GABA_A$ receptor-mediated currents in PNs.

Financial disclosures

None of the authors have any financial arrangements or potential conflicts of interest to report.

Acknowledgments

I thank Dr. Hiroki Takei for his preliminary experiment. VGAT-Venus transgenic rats were generated by Drs. Y. Yanagawa, M. Hirabayashi and Y. Kawaguchi in the National Institute for Physiological Sciences, Okazaki, Japan, using pCS2-Venus provided by Dr. A. Miyawaki.

I am grateful to Prof. Yoshiyuki Oi for the opportunity to perform this study, Prof. Masayuki Kobayashi for their instructions of this study, and colleagues in Department of Pharmacology for their technical advice and assistance.

References

Almado, C.E.L., Machado, B.H., Leao, R.M., 2012. Chronic intermittent hypoxia depresses afferent neurotransmission in NTS neurons by a reduction in the number of active synapses. J. Neurosci. 32, 16736–16746.

Ammoun, S., Holmqvist, T., Shariatmadari, R., Oonk, H.B., Detheux, M., Parmentier, M., Åkerman, K.E.O., Kukkonen, J.P., 2003. Distinct recognition of OX1 and OX2 receptors by orexin peptides. J. Pharmacol. Exp. Therapeut. 305, 507–514.

Aracri, P., Banfi, D., Pasini, M.E., Amadeo, A., Becchetti, A., 2015. Hypocretin (orexin) regulates glutamate input to fast-spiking interneurons in layer V of the Fr2 region of the murine prefrontal cortex. Cerebr. Cortex 25, 1330–1347.

Azhdari Zarmehri, H., Semnanian, S., Fathollahi, Y., Erami, E., Khakpay, R., Azizi, H., Rohampour, K., 2011. Intra-periaqueductal gray matter microinjection of orexin-A decreases formalin-induced nociceptive behaviors in adult male rats. J. Pain 12, 280–287.

Bahaaddini, M., Khatamsaz, S., Esmaeili-Mahani, S., Abbasnejad, M., Raoof, M., 2016. The role of trigeminal nucleus caudalis orexin 1 receptor in orofacial pain-induced anxiety in rat. Neuroreport 27, 1107–1113.

Bartsch, T., Levy, M.J., Knight, Y.E., Goadsby, P.J., 2004. Differential modulation of nociceptive dural input to [hypocretin] orexin A and B receptor activation in the posterior hypothalamic area. Pain 109, 367–378.

Bayer, L., Eggermann, E., Saint-Mleux, B., Machard, D., Jones, B.E., Mühlethaler, M., Serafin, M., 2002. Selective action of orexin (hypocretin) on nonspecific thalamocortical projection neurons. J. Neurosci. 22, 7835–7839.

Berridge, M.J., 1998. Neuronal calcium signaling. Neuron 21, 13–26.

Bingham, S., Davey, P.T., Babbs, A.J., Irving, E.A., Sammons, M.J., Wyles, M., Jeffrey, P., Cutler, L., Riba, I., Johns, A., Porter, R.A., Upton, N., Hunter, A.J., Parsons, A.A., 2001. Orexin-A, an hypothalamic peptide with analgesic properties. Pain 92, 81–90.

Brandon, N., Jovanovic, J., Moss, S., 2002. Multiple roles of protein kinases in the modulation of gamma-aminobutyric acidA receptor function and cell surface expression. Pharmacol. Ther. 94, 113–122.

Brandon, N.J., Delmas, P., Kittler, J.T., McDonald, B.J., Sieghart, W., Brown, D.A., Smart, T.G., Moss, S.J., 2000. $GABA_A$ receptor phosphorylation and functional modulation in cortical neurons by a protein kinase C-dependent pathway. J. Biol. Chem. 275, 38856–38862.

Burkey, A.R., Carstens, E., Wenniger, J.J., Tang, J., Jasmin, L., 1996. An opioidergic cortical antinociception triggering site in the agranular insular cortex of the rat that contributes to morphine antinociception. J. Neurosci. 16, 6612–6623.

Cheng, J.-K., Chou, R.C.-C., Hwang, L.-L., Chiou, L.-C., 2003. Antiallodynic effects of intrathecal orexins in a rat model of postoperative pain. J. Pharmacol. Exp. Therapeut. 307, 1065–1071.

Craig, A.D., Chen, K., Bandy, D., Reiman, E.M., 2000. Thermosensory activation of insular cortex. Nat. Neurosci. 3, 184–190.

Davis, S., Williams, K., Xu, W., Glatzer, N.R., Smith, B.N., 2003. Selective enhancement of synaptic inhibition by hypocretin (orexin) in rat vagal motor neurons: implications for autonomic regulation. J. Neurosci. 23, 3844–3854.

de Lecea, L., Kilduff, T.S., Peyron, C., Gao, X., Foye, P.E., Danielson, P.E., Fukuhara, C., Battenberg, E.L., Gautvik, V.T., Bartlett, F.S., Frankel, W.N., van den Pol, A.N., Bloom, F.E., Gautvik, K.M., Sutcliffe, J.G., 1998. The hypocretins: hypothalamusspecific peptides with neuroexcitatory activity. Proc. Natl. Acad. Sci. U. S. A. 95, 322–327.

Deleuze, C., Huguenard, J.R., 2006. Distinct electrical and chemical connectivity maps in the thalamic reticular nucleus: potential roles in synchronization and sensation. J. Neurosci. 26, 8633–8645.

Dergacheva, O., Bateman, R., Byrne, P., Mendelowitz, D., 2012. Orexinergic modulation of GABAergic neurotransmission to cardiac vagal neurons in the brain stem nucleus ambiguus changes during development. Neuroscience 209, 12–20

Galarreta, M., Hestrin, S., 2002. Electrical and chemical synapses among parvalbumin fast-spiking GABAergic interneurons in adult mouse neocortex. Proc. Natl. Acad. Sci. U. S. A. 99, 12438–12443.

Grundy, D., 2015. Principles and standards for reporting animal experiments in the journal of physiology and experimental physiology. J. Physiol. 593, 2547–2549.

Ho, Y.-C., Lee, H.-J., Tung, L.-W., Liao, Y.-Y., Fu, S.-Y., Teng, S.-F., Liao, H.-T., Mackie, K., Chiou, L.-C., 2011. Activation of orexin 1 receptors in the periaqueductal gray of male rats leads to antinociception via retrograde endocannabinoid (2-arachidonoylglycerol)-induced disinhibition. J. Neurosci. 31, 14600–14610.

Hollander, J.A., Lu, Q., Cameron, M.D., Kamenecka, T.M., Kenny, P.J., 2008. Insular hypocretin transmission regulates nicotine reward. Proc. Natl. Acad. Sci. U. S. A. 105, 19480–19485.

Holmqvist, T., Åkerman, K.E., Kukkonen, J.P., 2001. High specificity of human orexin receptors for orexins over neuropeptide Y and other neuropeptides. Neurosci. Lett. 305, 177–180.

Horinuki, E., Shinoda, M., Shimizu, N., Koshikawa, N., Kobayashi, M., 2015. Orthodontic force facilitates cortical responses to periodontal stimulation. J. Dent. Res. 94, 1158–1166.

Inutsuka, A., Yamashita, A., Chowdhury, S., Nakai, J., Ohkura, M., Taguchi, T., Yamanaka, A., 2016. The integrative role of orexin/hypocretin neurons in nociceptive perception and analgesic regulation. Sci. Rep. 6, 29480.

Jasmin, L., Boudah, A., Ohara, P.T., 2003. Long-term effects of decreased noradrenergic central nervous system innervation on pain behavior and opioid antinociception. J. Comp. Neurol. 460, 38–55.

Kajiyama, S., Kawamoto, M., Shiraishi, S., Gaus, S., Matsunaga, A., Suyama, H., Yuge, O., 2005. Spinal orexin-1 receptors mediate anti-hyperalgesic effects of

intrathecally-administered orexins in diabetic neuropathic pain model rats. Brain Res. 1044, 76–86.

Kaneko, M., Horinuki, E., Shimizu, N., Kobayashi, M., 2017. Physiological profiles of cortical responses to mechanical stimulation of the tooth in the rat: an optical imaging study. Neuroscience 358, 170–180.

Katagiri, A., Okamoto, K., Thompson, R., Rahman, M., Bereiter, D.A., 2014. Posterior hypothalamic modulation of ocular-responsive trigeminal subnucleus caudalis neurons is mediated by Orexin-A and Orexin1 receptors. Eur. J. Neurosci. 40, 2619–2627.

Kawaguchi, Y., Kubota, Y., 1997. GABAergic cell subtypes and their synaptic connections in rat frontal cortex. Cerebr. Cortex 7, 476–486.

Kenny, P.J., 2011. Tobacco dependence, the insular cortex and the hypocretin connection. Pharmacol. Biochem. Behav. 97, 700–707.

Kittler, J.T., Moss, S.J., 2003. Modulation of $GABA_A$ receptor activity by phosphorylation and receptor trafficking: implications for the efficacy of synaptic inhibition. Curr. Opin. Neurobiol. 13, 341–347.

Kobayashi, M., Fujita, S., Takei, H., Song, L., Chen, S., Suzuki, I., Yoshida, A., Iwata, K., Koshikawa, N., 2010. Functional mapping of gustatory neurons in the insular cortex revealed by pERK-immunohistochemistry and in vivo optical imaging. Synapse 64, 323–334.

Koyanagi, Y., Oi, Y., Yamamoto, K., Koshikawa, N., Kobayashi, M., 2014. Fast-spiking cell to pyramidal cell connections are the most sensitive to propofol-induced facilitation of GABAergic currents in rat insular cortex. Anesthesiology 121, 68–78.

Koyanagi, Y., Yamamoto, K., Oi, Y., Koshikawa, N., Kobayashi, M., 2010. Presynaptic interneuron subtype- and age-dependent modulation of GABAergic synaptic transmission by β-adrenoceptors in rat insular cortex. J. Neurophysiol. 103, 2876–2888.

Kubota, Y., Karube, F., Nomura, M., Kawaguchi, Y., 2016. The diversity of cortical inhibitory synapses. Front. Neural Circuits 10, 27.

Lai, X., Ye, L., Liao, Y., Jin, L., Ma, Q., Lu, B., Sun, Y., Shi, Y., Zhou, N., 2016. Agonistinduced activation of histamine H3 receptor signals to extracellular signal-regulated kinases 1 and 2 through PKC-, PLD-, and EGFR-dependent mechanisms. J. Neurochem. 137, 200–215.

Lambe, E.K., Liu, R.-J., Aghajanian, G.K., 2007. Schizophrenia, hypocretin (orexin), and the thalamocortical activating system. Schizophr. Bull. 33, 1284–1290.

Marcus, J.N., Aschkenasi, C.J., Lee, C.E., Chemelli, R.M., Saper, C.B., Yanagisawa, M., Elmquist, J.K., 2001. Differential expression of orexin receptors 1 and 2 in the rat brain. J. Comp. Neurol. 435, 6–25.

Nagai, T., Ibata, K., Park, E.S., Kubota, M., Mikoshiba, K., Miyawaki, A., 2002. A variant of yellow fluorescent protein with fast and efficient maturation for cell-biological applications. Nat. Biotechnol. 20, 87–90.

Nakamura, H., Kato, R., Shirakawa, T., Koshikawa, N., Kobayashi, M., 2015. Spatiotemporal profiles of dental pulp nociception in rat cerebral cortex: an optical imaging study. J. Comp. Neurol. 523, 1162–1174.

Nakamura, H., Shirakawa, T., Koshikawa, N., Kobayashi, M., 2016. Distinct excitation to pulpal stimuli between somatosensory and insular cortices. J. Dent. Res. 95, 180–187.

Nambu, T., Sakurai, T., Mizukami, K., Hosoya, Y., Yanagisawa, M., Goto, K., 1999. Distribution of orexin neurons in the adult rat brain. Brain Res. 827, 243–260.

Naqvi, N.H., Rudrauf, D., Damasio, H., Bechara, A., 2007. Damage to the insula disrupts addiction to cigarette smoking. Science 315, 531–534.

Nusser, Z., Sieghart, W., Mody, I., 1999. Differential regulation of synaptic $GABA_A$ receptors by cAMP-dependent protein kinase in mouse cerebellar and olfactory bulb neurones. J. Physiol. 521 Pt 2, 421–435.

Peyron, C., Tighe, D.K., van den Pol, A.N., de Lecea, L., Heller, H.C., Sutcliffe, J.G., Kilduff, T.S., 1998. Neurons containing hypocretin (orexin) project to multiple neuronal systems. J. Neurosci. 18, 9996–10015.

Pi, H.-J., Hangya, B., Kvitsiani, D., Sanders, J.I., Huang, Z.J., Kepecs, A., 2013. Cortical interneurons that specialize in disinhibitory control. Nature 503, 521–524.

Plaza-Zabala, A., Flores, Á., Martín-García, E., Saravia, R., Maldonado, R., Berrendero, F., 2013. A role for hypocretin/orexin receptor-1 in cue-induced reinstatement of nicotine-seeking behavior. Neuropsychopharmacology 38, 1724–1736.

Poisbeau, P., Cheney, M.C., Browning, M.D., Mody, I., 1999. Modulation of synaptic $GABA_A$ receptor function by PKA and PKC in adult hippocampal neurons. J. Neurosci. 19, 674–683.

Sah, P., 1996. Ca^{2+}-activated K^+ currents in neurones: types, physiological roles and modulation. Trends Neurosci. 19, 150–154.

Sakurai, T., 2007. The neural circuit of orexin (hypocretin): maintaining sleep and wakefulness. Nat. Rev. Neurosci. 8, 171–181.

Sakurai, T., Amemiya, A., Ishii, M., Matsuzaki, I., Chemelli, R.M., Tanaka, H., Williams, S.C., Richardson, J.A., Kozlowski, G.P., Wilson, S., Arch, J.R., Buckingham, R.E., Haynes, A.C., Carr, S.A., Annan, R.S., McNulty, D.E., Liu, W.S., Terrett, J.A., Elshourbagy, N.A., Bergsma, D.J., Yanagisawa, M., 1998. Orexins and orexin receptors: a family of hypothalamic neuropeptides and G protein-coupled receptors that regulate feeding behavior. Cell 92, 573–585.

Schönwasser, D.C., Marais, R.M., Marshall, C.J., Parker, P.J., 1998. Activation of the mitogen-activated protein kinase/extracellular signal-regulated kinase pathway by conventional, novel, and atypical protein kinase C isotypes. Mol. Cell Biol. 18, 790–798.

Sun, X., Gu, X.Q., Haddad, G.G., 2003. Calcium influx via L- and N-type calcium channels activates a transient large-conductance Ca^{2+}-activated K^+ current in mouse neocortical pyramidal neurons. J. Neurosci. 23, 3639–3648.

Sutcliffe, J.G., de Lecea, L., 2002. The hypocretins: setting the arousal threshold. Nat. Rev. Neurosci. 3, 339–348.

Takei, H., Yamamoto, K., Bae, Y.-C., Shirakawa, T., Kobayashi, M., 2017. Histamine H_3 heteroreceptors suppress glutamatergic and GABAergic synaptic transmission in the rat insular cortex. Front. Neural Circuits 11, 85.

Uematsu, M., Hirai, Y., Karube, F., Ebihara, S., Kato, M., Abe, K., Obata, K., Yoshida, S., Hirabayashi, M., Yanagawa, Y., Kawaguchi, Y., 2008. Quantitative chemical composition of cortical GABAergic neurons revealed in transgenic venus-expressing rats. Cerebr. Cortex 18, 315–330.

Yamamoto, K., Koyanagi, Y., Koshikawa, N., Kobayashi, M., 2010a. Postsynaptic cell type–dependent cholinergic regulation of GABAergic synaptic transmission in rat insular cortex. J. Neurophysiol. 104, 1933–1945.

Yamamoto, K., Noguchi, J., Yamada, C., Watabe, A.M., Kato, F., 2010b. Distinct target cell-dependent forms of short-term plasticity of the central visceral afferent synapses of the rat. BMC Neurosci. 11, 134.

Yamamoto, T., Nozaki-Taguchi, N., Chiba, T., 2002. Analgesic effect of intrathecally administered orexin-A in the rat formalin test and in the rat hot plate test. Br. J. Pharmacol. 137, 170–176.

Yamamoto, T., Saito, O., Shono, K., Hirasawa, S., 2003. Activation of spinal orexin-1 receptor produces anti-allodynic effect in the rat carrageenan test. Eur. J. Pharmacol. 481, 175–180.

Yamamoto, T., Yuyama, N., Kato, T., Kawamura, Y., 1984. Gustatory responses of cortical neurons in rats. I. Response characteristics. J. Neurophysiol. 51, 616–635.

Yamamoto, K., Kobayashi, M., 2018. Opposite roles in short-term plasticity for N-type and P/Q-Type voltage-dependent calcium channels in GABAergic neuronal connections in the rat cerebral cortex. J. Neurosci. 38, 9814–9828.

Yasui, Y., Breder, C.D., Safer, C.B., Cechetto, D.F., 1991. Autonomic responses and efferent pathways from the insular cortex in the rat. J. Comp. Neurol. 303, 355–374.

Zhu, Y., Miwa, Y., Yamanaka, A., Yada, T., Shibahara, M., Abe, Y., Sakurai, T., Goto, K., 2003. Orexin receptor type-1 couples exclusively to pertussis toxin-insensitive Gproteins, while orexin receptor type-2 couples to both pertussis toxin-sensitive and -insensitive G-proteins. J. Pharmacol. Sci. 92, 259–266.

Figures

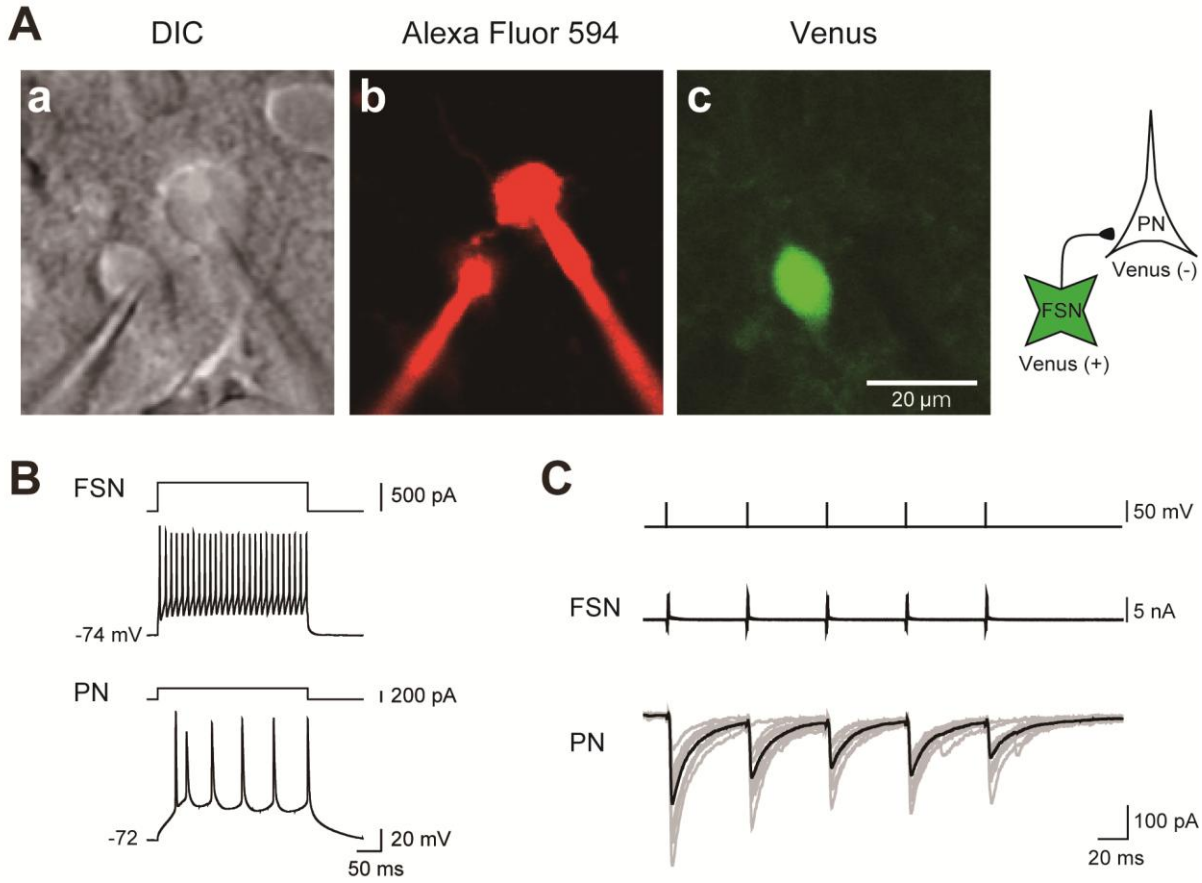

Fig. 1. Paired whole-cell patch-clamp recording of inhibitory connections from a fast-spiking neuron (FSN) to a pyramidal neuron (PN) in layer V of the insular cortex (IC). (A) Paired whole-cell patch-clamp recordings were performed under differential interference contrast infrared video microscopy (DIC; a). Red and green fluorescent images indicate Alexa Fluor 594 added into the internal solution to visualize somatic and dendritic shapes of recorded neurons (b) and a vesicular GABA transporter (VGAT)-Venus positive neuron (Venus; c), respectively. (B) Repetitive spike firing induced by depolarizing current pulse injection (300 ms) recorded from Venus-positive and Venus-negative neurons. The upper neuron was identified as an FSN based on a large and fast afterhyperpolarization (AHP) and high-frequency spike firing without spike adaptation. The PN was characterized by a Venus-negative soma and spike firing with adaptation. Resting membrane potentials are shown to the left of the traces. (C) Short depolarizing voltage-pulse injection induced action currents in the FSN, which elicited unitary IPSCs (uIPSCs) in the PN. Holding potential (Vh) was set at −60 mV. Ten consecutive traces (gray) were superimposed with averaged traces (black).

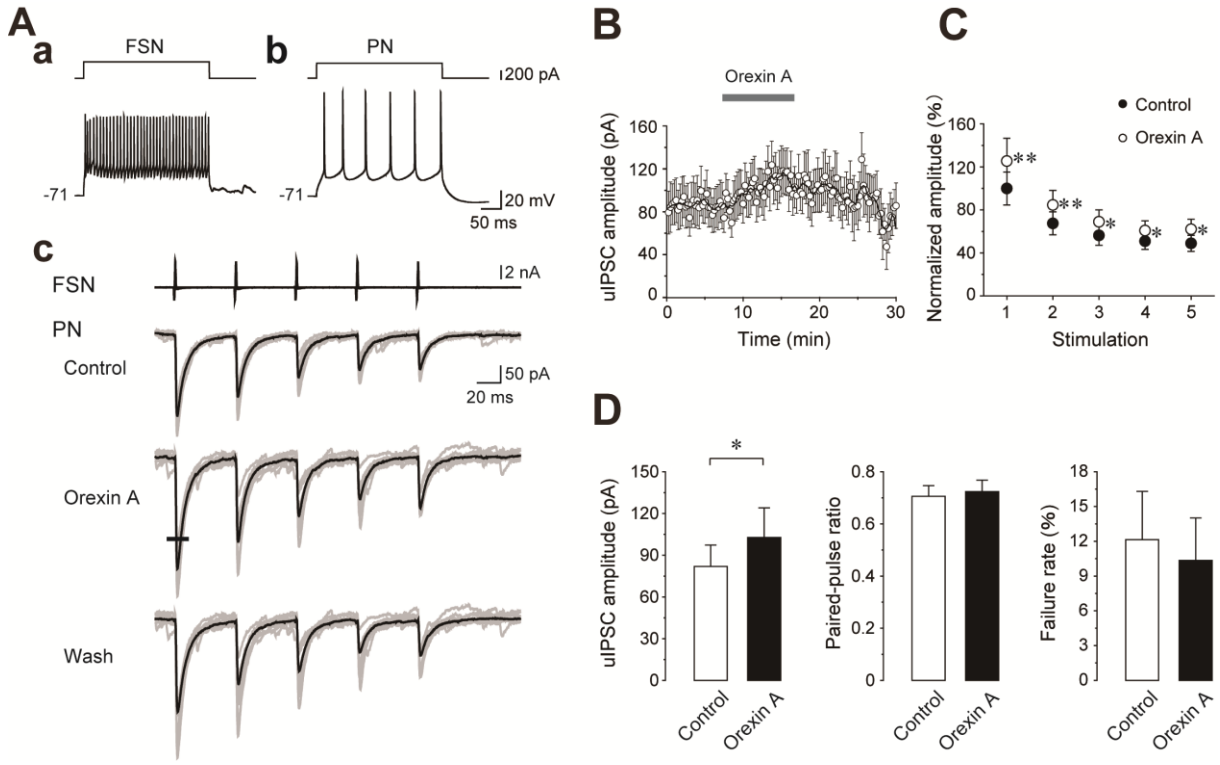

Fig. 2. Facilitative effects of orexin A on uIPSCs in an FSN-to-PN (FSN→PN) connection. (A) uIPSC recording from an FSN→PN connection. Suprathreshold voltage responses (lower traces) of an FSN (a) and a PN (b) in response to depolarizing current pulse injection (upper traces). uIPSC recordings from the PN responding to action currents (top traces) induced by an injection of short (2 ms, +80 mV) train pulses (5 pulses at 20 Hz) to the FSN (c). Ten consecutive traces (gray) and their average traces (black) are superimposed. Note that uIPSC amplitude was enhanced by application of 100 nM orexin A. The facilitative effect of orexin A was reversible (Wash, bottom traces). A horizontal bar shown in the traces of orexin A indicates the same amplitude of the mean in the control condition. (B) The uIPSC amplitude before, during, and after 100 nM orexin A application in the FSN→PN connection shown in (A) is plotted against time. The solid line indicates the moving average line of 5 points. (C) The normalized amplitude of the 1st to 5th uIPSCs in control (filled circles) and orexin A application (open circles). (D) Summary of orexin A-induced effects on uIPSC amplitude, paired-pulse ratio, and failure rate in FSN→PN connections (orexin A, n = 28). *P < 0.05, paired *t*-test.

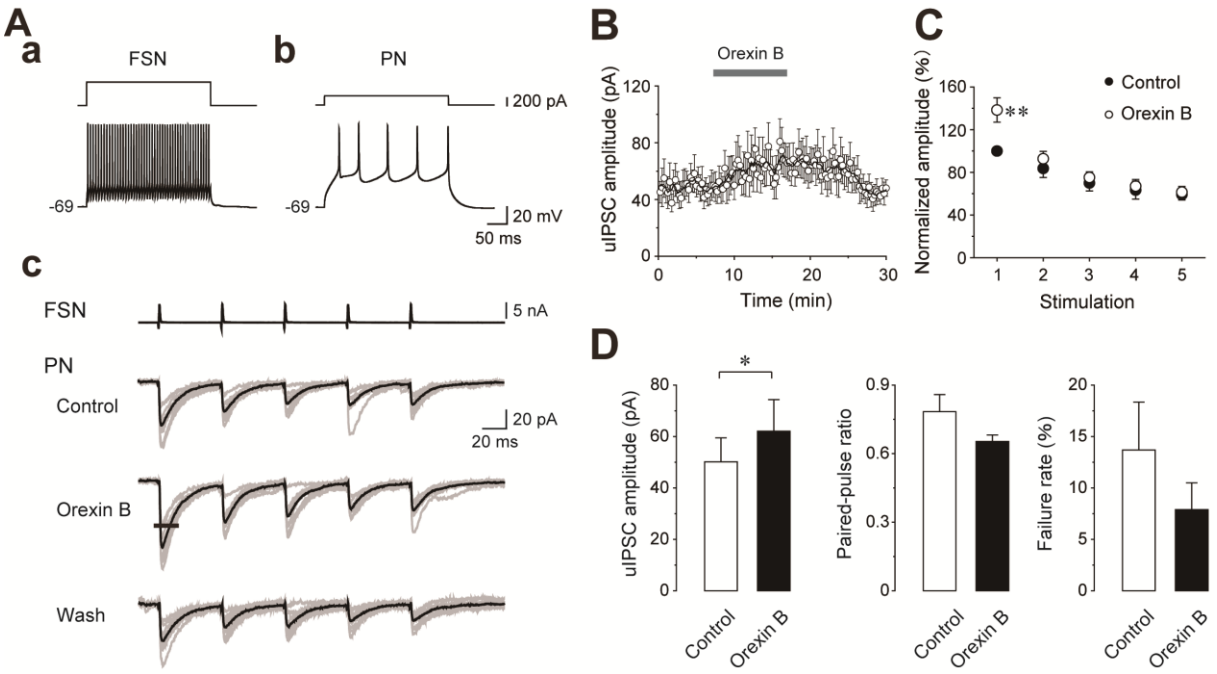

Fig. 3. Facilitative effects of orexin B on uIPSCs in FSN→PN connections. (A) uIPSC recordings in an FSN→PN connection. Suprathreshold voltage responses of an FSN (a) and a PN (b) in response to depolarizing current pulse injection. uIPSC amplitude was enhanced by application of 100 nM orexin B (c). (B) Time course of the uIPSC amplitude before, during, and after 100 nM orexin B application in the FSN→PN connection shown in (A). (C) The normalized amplitude of the 1st to 5th uIPSCs in control and orexin B application. (D) Orexin B increased uIPSC amplitude without affecting paired-pulse ratio or failure rate in FSN→PN connections (n = 19). *P < 0.05, paired *t*-test.

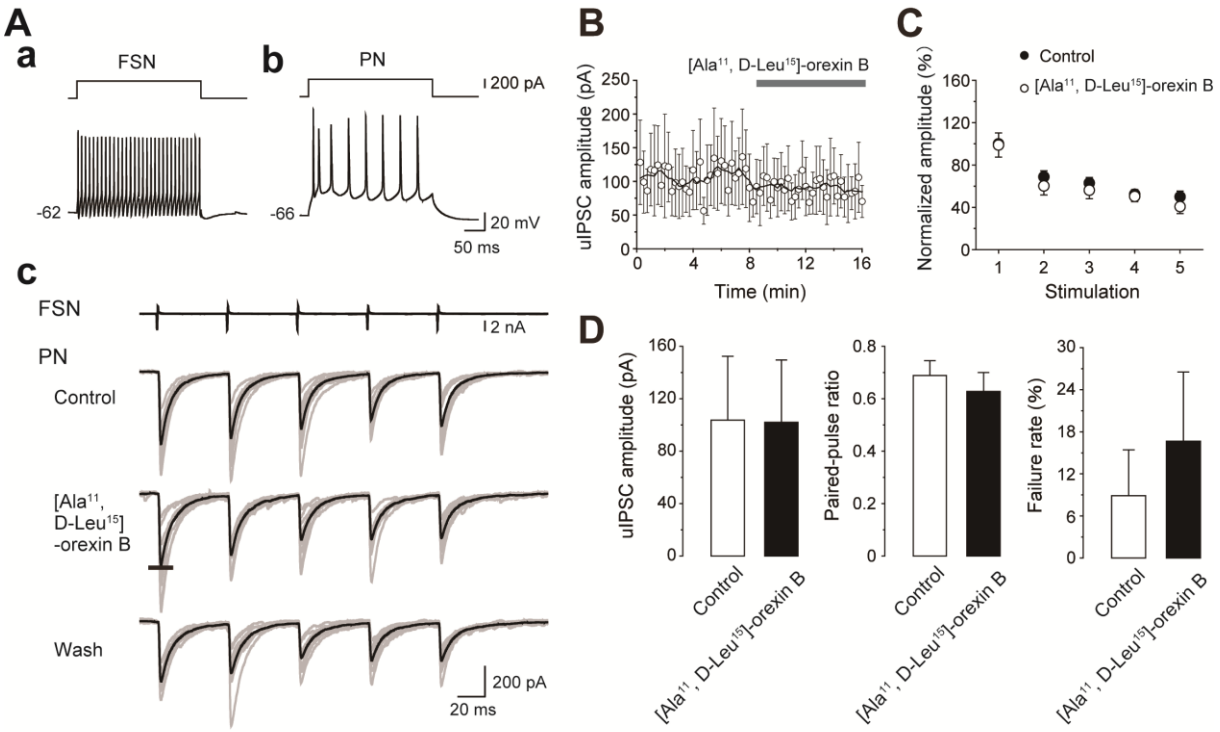

Fig. 4. Little effect of 1 μM [Ala^{11}, D-Leu^{15}]-orexin B, a selective orexinergic receptor 2 (OX_2R) agonist, on uIPSCs in FSN→PN connections. (A) Repetitive spike firing patterns of an FSN (a) and a PN (b) and uIPSCs obtained from an FSN→PN connection before (control), during, and after (wash) bath application of [Ala^{11}, D-Leu^{15}]-orexin B (c). Note the little effect of [Ala^{11}, D-Leu^{15}]-orexin B on uIPSCs. (B) Time course of the uIPSC amplitude before, during, and after 1 μM [Ala^{11}, D-Leu^{15}]-orexin B application in the FSN→PN connection shown in (A). (C) The normalized amplitude of the 1st to 5th uIPSCs in control and during [Ala^{11}, D-Leu^{15}]-orexin B application. (D) Summary of the effects of [Ala^{11}, D-Leu^{15}]-orexin B on uIPSC amplitude, paired-pulse ratio, and failure rate in FSN→PN connections (n = 9).

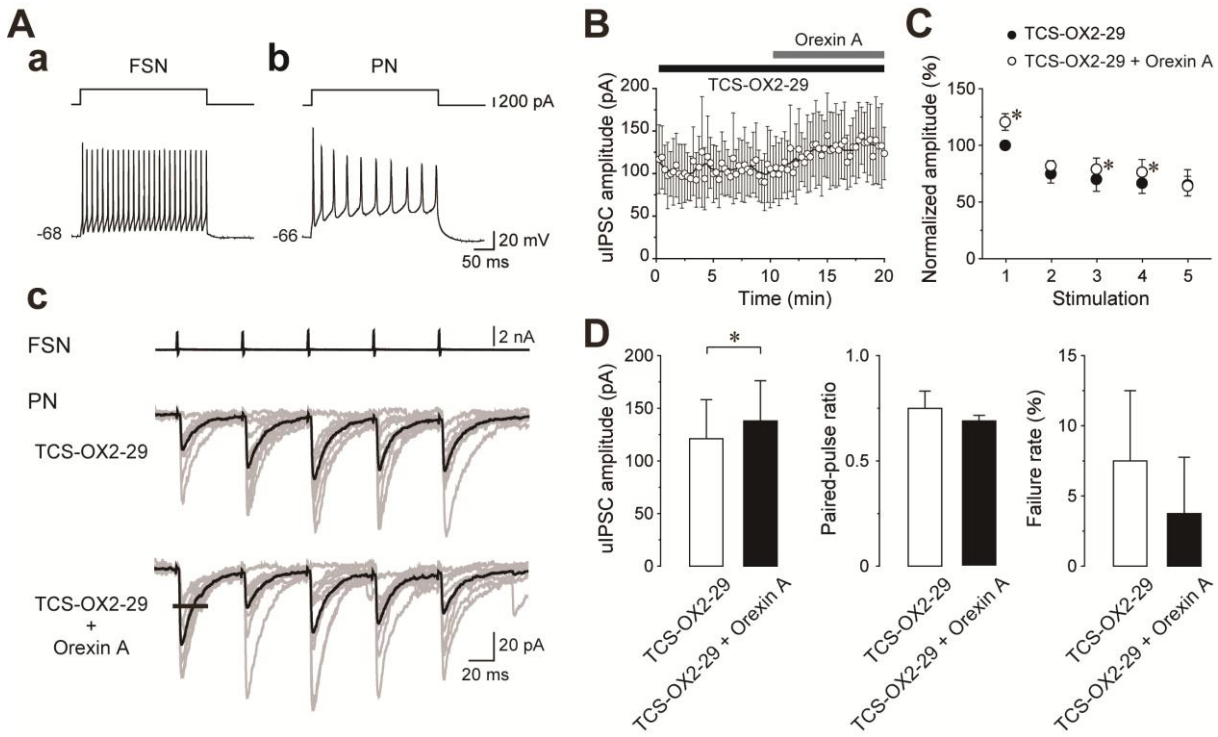

Fig. 5. Orexin A (100 nM) enhances uIPSCs in the presence of 10 μM TCS-OX2-29, a selective OX_2R antagonist, in FSN→PN connections. (A) Repetitive spike firing of an FSN (a) and a PN (b). Orexin A enhanced uIPSCs under TCS-OX2-29 application (c). (B) Time course of uIPSC amplitude before and during orexin A application in the FSN→PN connection shown in (A). (C) The normalized amplitude of the 1st to 5th uIPSCs during application of orexin A with TCS-OX2-29. (D) Summary of orexin A-induced effects in combination with TCS-OX2-29 on uIPSC amplitude, paired-pulse ratio, and failure rate in FSN→PN connections (n = 8). *P < 0.05, paired *t*-test.

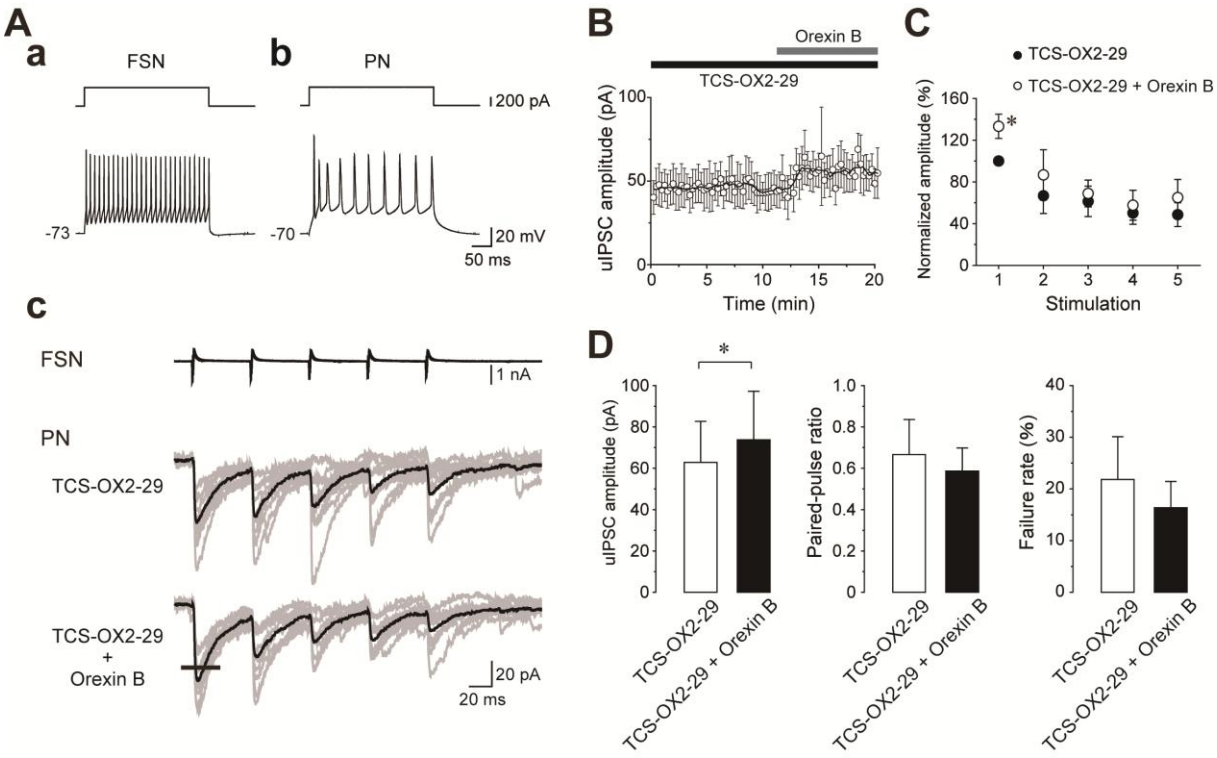

Fig. 6. Orexin B (100 nM) enhances uIPSCs in the presence of 10 μM TCS-OX2-29 in FSN→PN connections. (A) Repetitive spike firing of an FSN (a) and a PN (b). Orexin B enhanced uIPSCs under TCS-OX2-29 application (c). (B) Time course of uIPSC amplitude before and during orexin B application in the FSN→PN connection shown in (A). (C) The normalized amplitude of the 1st to 5th uIPSCs during application of orexin B with TCS-OX2-29. (D) Summary of orexin B-induced effects in combination with TCS-OX2-29 on uIPSC amplitude, paired-pulse ratio, and failure rate in FSN→PN connections (n = 11). *P < 0.05, paired *t*-test.

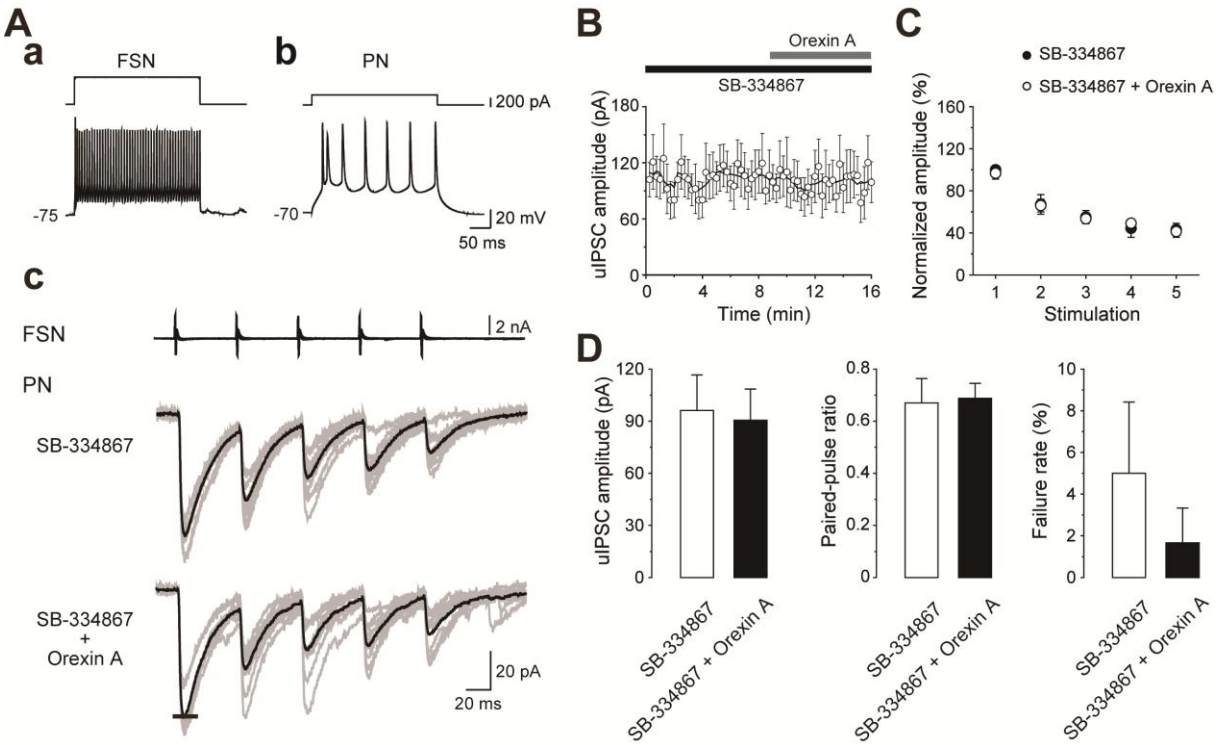

Fig. 7. SB-334867, a selective orexinergic receptor 1 (OX_1R) antagonist, blocks the orexin A-induced enhancement of uIPSCs in FSN→PN connections. (A) Suprathreshold voltage responses of an FSN (a) and a PN (b) in response to depolarizing current pulse injection. uIPSC recordings in the FSN→PN connection under application of 10 μM SB-334867 and 100 nM orexin A (c). Note the little effect of orexin A on uIPSC amplitude when applied with SB-334867. (B) Time course of uIPSC amplitude before and during orexin A application under preapplication of SB-334867 in the FSN→PN connection shown in (A). (C) The normalized amplitude of the 1st to 5th uIPSCs under application of SB-334867 and orexin A. (D) Summary of orexin A-induced effects in combination with SB-334867 on uIPSC amplitude, paired-pulse ratio, and failure rate in FSN→PN connections (n = 7).

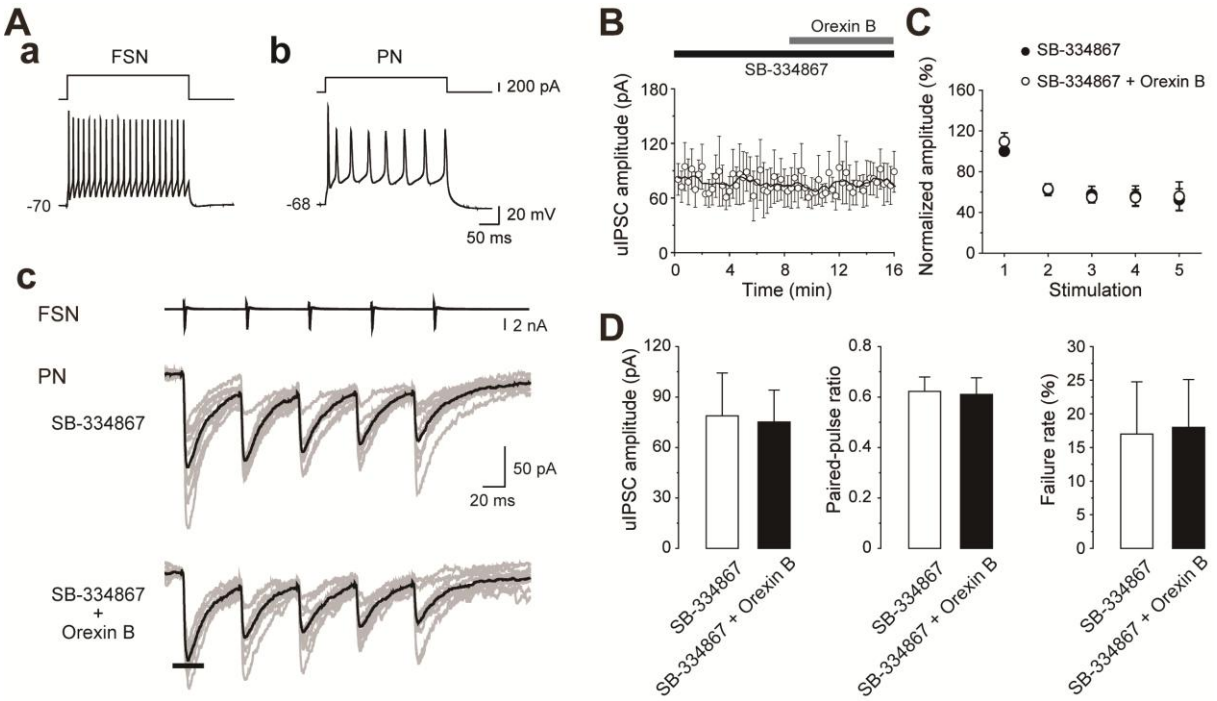

Fig. 8. SB-334867 blocks the orexin B-induced enhancement of uIPSCs FSN→PN connections. (A) Repetitive spike firing of an FSN (a) and a PN (b) in response to depolarizing current pulse injection. uIPSC recordings in the FSN→PN connection under application of 10 μM SB-334867 and 100 nM orexin B. Note the little effect of orexin B on uIPSC amplitude applied with SB-334867. (B) Time course of uIPSC amplitude before and during orexin B application under preapplication of SB-334867 in the FSN→PN connection shown in (A). (C) The normalized amplitude of the 1st to 5th uIPSCs under application of SB-334867 and orexin B. (D) Summary of orexin B-induced effects in combination with SB-334867 on uIPSC amplitude, paired-pulse ratio, and failure rate in FSN→PN connections (n = 10).

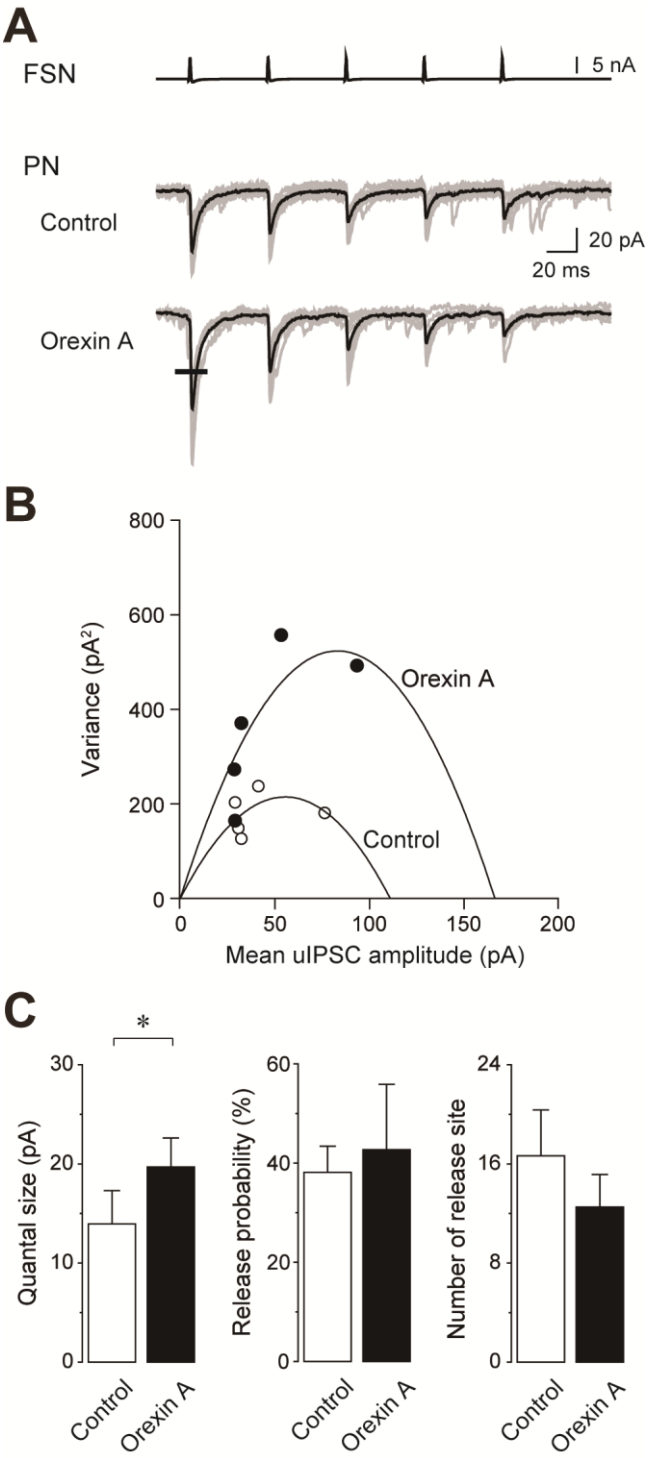

Fig. 9. Variance-mean analysis of uIPSCs in FSN→PN connections. (A) A representative example of variance-mean analysis of uIPSC amplitude obtained from responses to 5 train pulses (20 Hz). (B) Potted data showing the relationship between the mean IPSC amplitude and their variance in control and 100 nM orexin A application shown in (A) were fitted by quadratic functions.

(C) Summary of estimated quantal size, release probability, and the number of release sites in control and orexin A application (n = 18). Note that an enhancement of quantal size is observed after orexin A application, whereas the release probability and the number of release sites were unchanged by orexin A application. *P < 0.05, paired *t*-test.

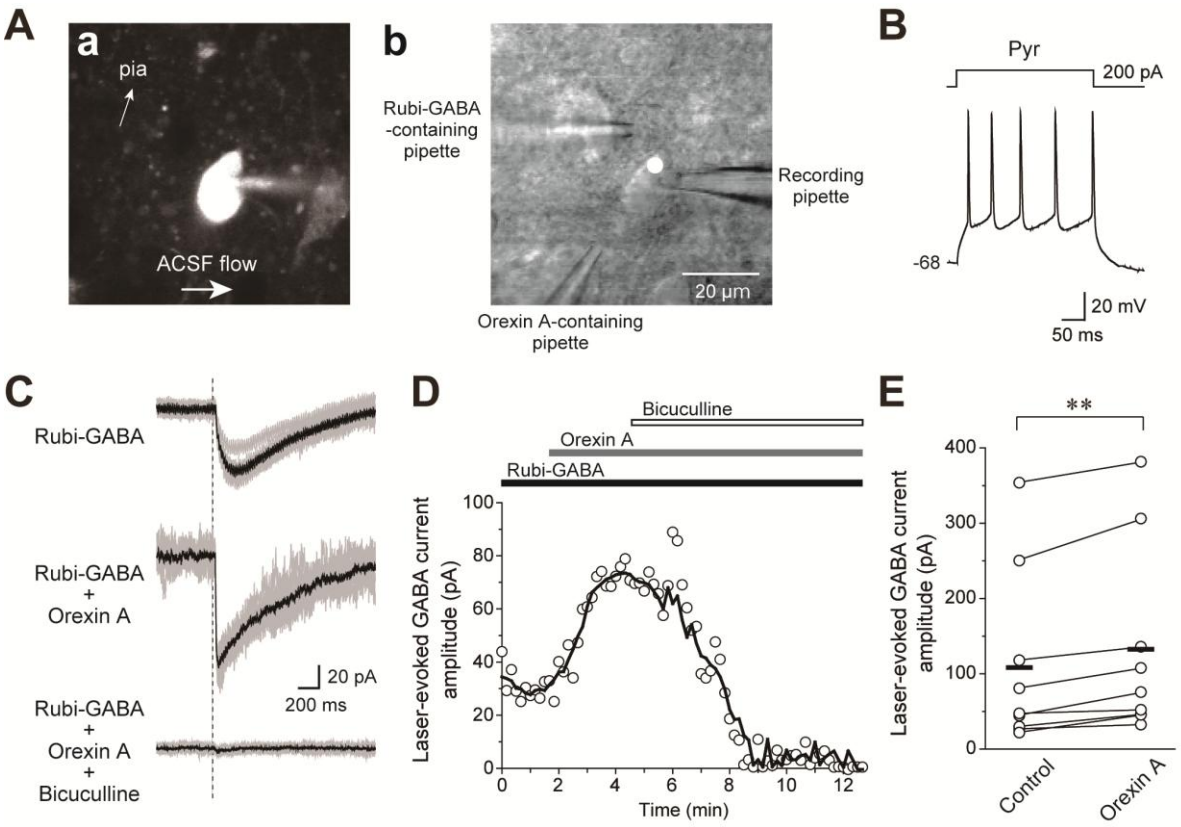

Fig. 10. Orexin A enhances the GABA-mediated currents induced by laser photolysis of ruthenium-bipyridine-triphenylphosphine-caged GABA (Rubi-GABA) recorded from PNs. (A) Whole-cell patch-clamp recording from a PN that was filled with Alexa Fluor 647 (a). Rubi-GABA (2 mM) and orexin A (100 nM) were applied from the pipettes placed upstream of the recorded PN (b). Location of laser photolysis is superimposed (open circle). (B) Repetitive spike firing of the PN. (C) Representative laser-evoked GABA-mediated currents (top) recorded from the PN shown in (A) and (B). Ten consecutive traces (gray) and their average traces (black) are superimposed. The vertical dotted line indicates the timing of photolysis with 473 nm laser. Tetrodotoxin (1 μM), D-AP5 (25 μM), and DNQX (40 μM) were applied in the perfusate. Note that continuous application of orexin A increased laser-evoked GABA currents (middle). Bath application of bicuculline (10 μM) diminished laser-evoked GABA currents (bottom). (D) Time course of the laser-evoked GABA current amplitude. The application periods of Rubi-GABA, orexin A with Rubi-GABA, and bicuculline with Rubi-GABA and orexin A are indicated on the top of the graph. (D) Summary of the effects of orexin A on the laser-evoked GABA currents (n = 9). Horizontal bars indicate the mean. **P < 0.01, paired *t*-test.

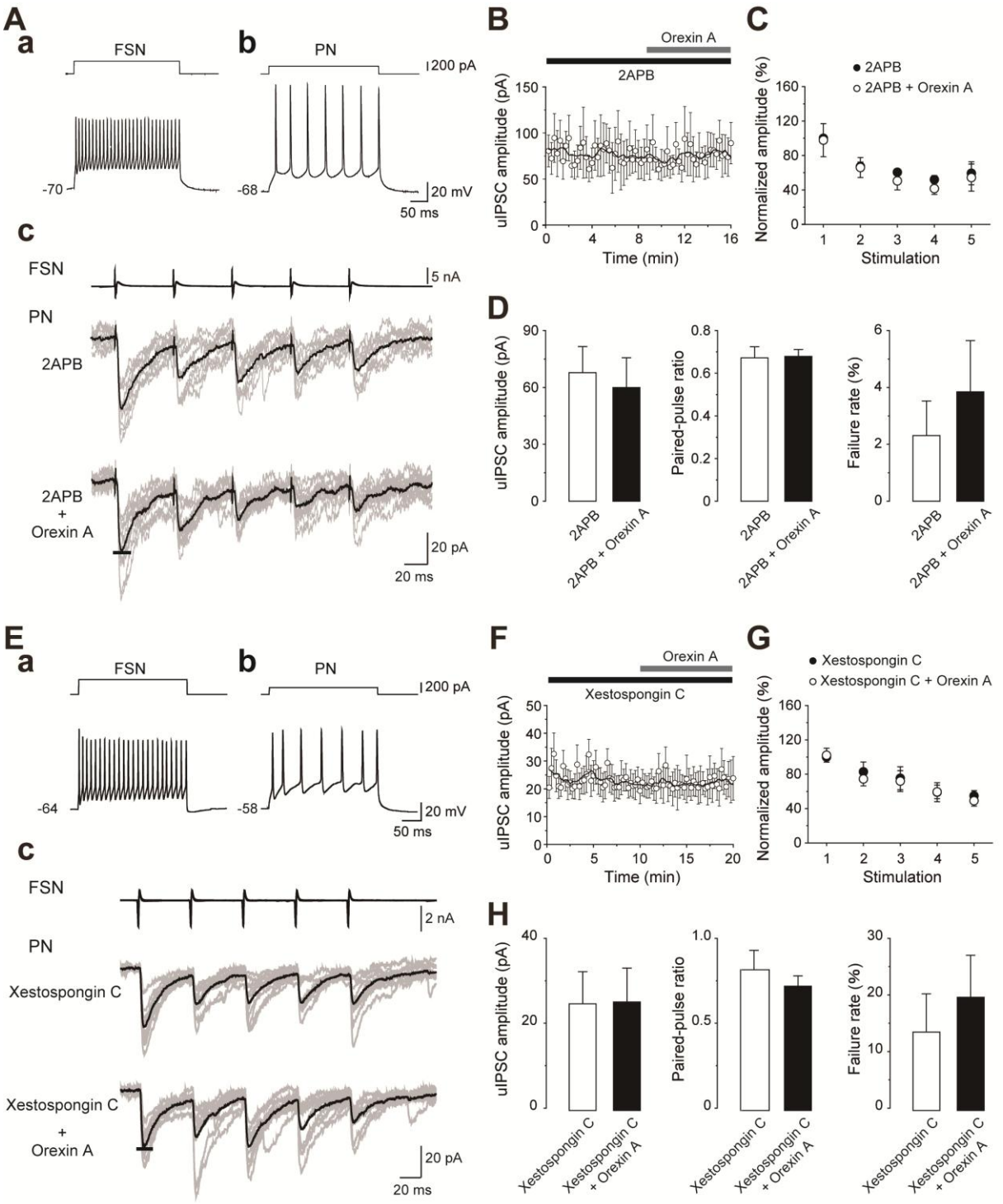

Fig. 11. Preapplication of the IP_3 receptor inhibitor, 2-aminoethoxydiphenyl borate (2APB) or xestospongin C, suppresses the orexin A-induced enhancement of uIPSCs in FSN→PN connections. (A) Repetitive spike firing of an FSN (a) and a PN (b). Orexin A (100 nM) had little effect on the amplitude of uIPSCs obtained from the FSN→PN connection under application of 15 μM 2APB (c). (B) Time course of uIPSC amplitude. The periods of 2APB and orexin A application are shown on the top. (C) The normalized amplitude of the 1st to 5th uIPSCs. (D) Summary of the effects of orexin A under application of 15 μM 2APB on uIPSC amplitude, paired-pulse ratio, and failure rate in FSN→PN connections (n = 13). (E) Repetitive spike firing of an FSN (a) and a PN (b). Orexin A had little effect on uIPSC amplitude obtained from the FSN→PN connection under application of 1 μM xestospongin C (c). (F) Time course of uIPSC amplitude. (G) The normalized amplitude of the 1st to 5th uIPSCs. (H) Summary of the effects of orexin A under application of xestospongin C on uIPSC amplitude, paired-pulse ratio, and failure rate in FSN→PN connections (n = 13).

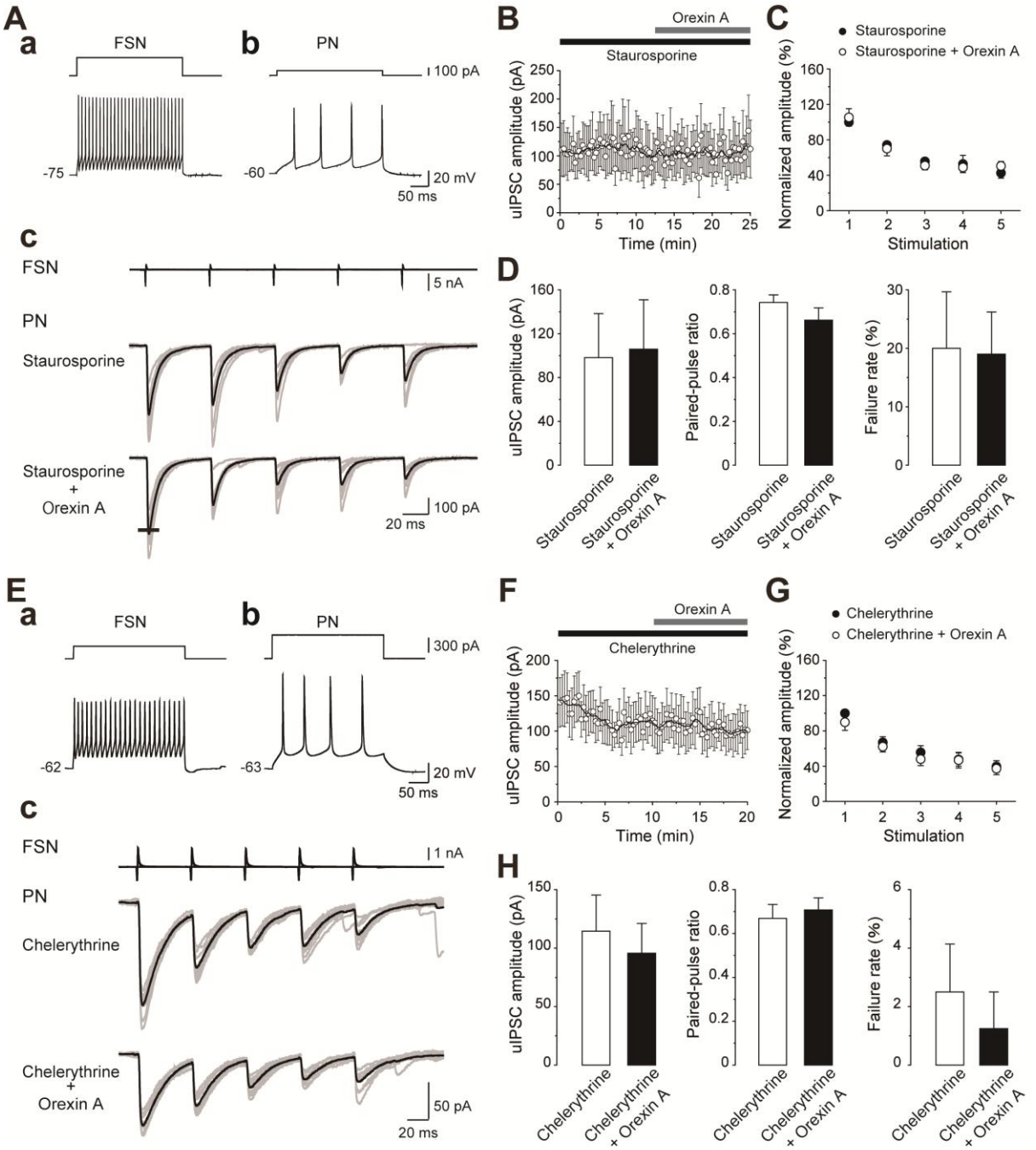

Fig. 12. Preapplication of the protein kinase C (PKC) inhibitor, staurosporine or chelerythrine, suppresses the orexin A-induced enhancement of uIPSCs in FSN→PN connections. (A) Repetitive spike firing of an FSN (a) and a PN (b). Orexin A (100 nM) had little effect on the amplitude of uIPSCs obtained from the FSN→PN connection under application of 1 μM staurosporine (c). (B) Time course of uIPSC amplitude. The periods of staurosporine and orexin A application are shown on the top. (C) The normalized amplitude of the 1st to 5th uIPSCs. (D) Summary of the effects of orexin A under application of 1 μM staurosporine on uIPSC amplitude, paired-pulse ratio, and failure rate in FSN→PN connections (n = 11). (E) Repetitive spike firing of an FSN (a) and a PN (b). Orexin A had little effect on uIPSC amplitude obtained from the FSN→PN connection under application of 1 μM chelerythrine (c). (F) Time course of uIPSC amplitude. (G) The normalized amplitude of the 1st to 5th uIPSCs. (H) Summary of the effects of orexin A under application of chelerythrine on uIPSC amplitude, paired-pulse ratio, and failure rate in FSN → PN connections (n = 8).

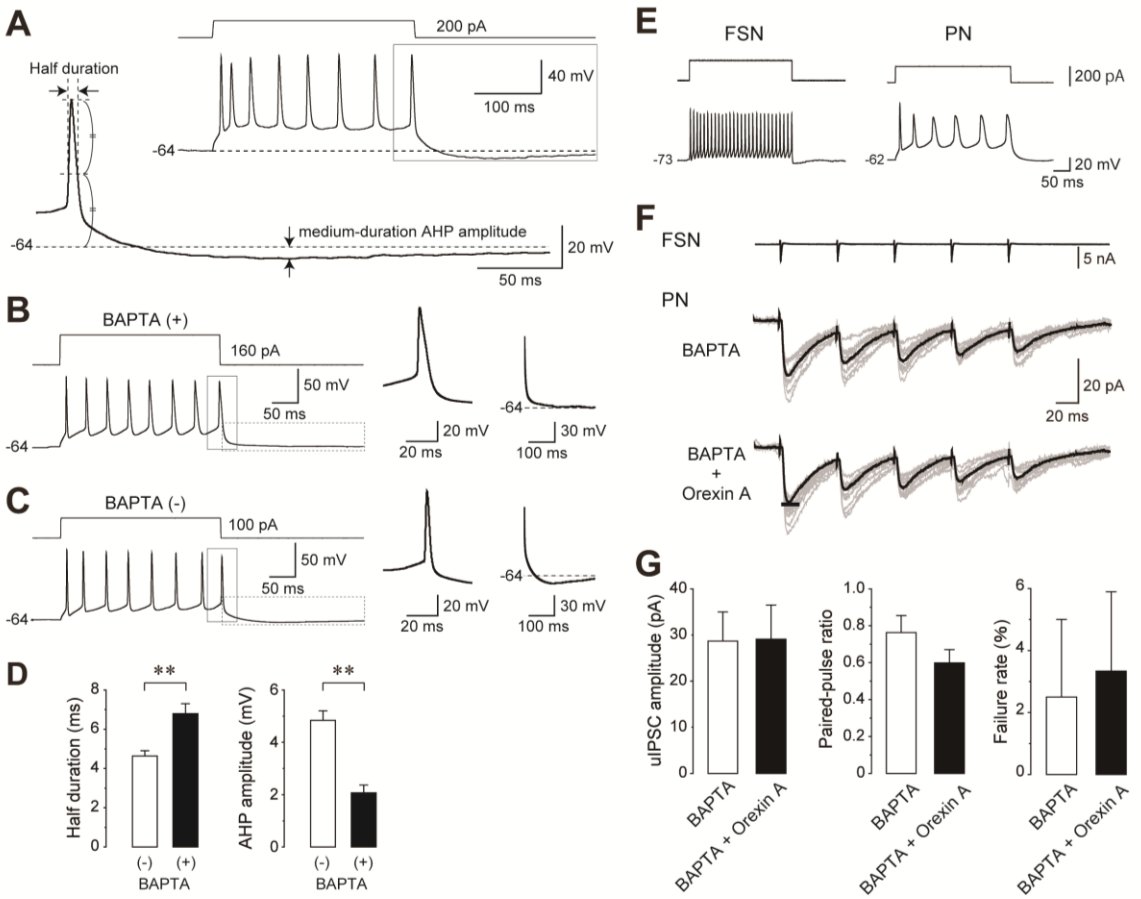

Fig. 13. Chelation of postsynaptic PN Ca^{2+} with BAPTA suppresses the orexin A-induced uIPSC enhancement in FSN→PN connections. (A) Repetitive spike firing of a PN. The last (8th) action potential is expanded to show how to measure the half-duration of the spike and medium-duration AHP amplitude. (B, C) Spike firing properties recorded using intracellular patch solutions with (B) and without BAPTA (C), respectively. The 8th spikes and following medium-duration AHP are expanded in the middle and right panels, respectively. Note the longer half duration and smaller medium-duration AHP amplitude in recording with BAPTA than those without BAPTA. (D) Summary of the effect of BAPTA on half duration of the 8th spikes and amplitude of medium-duration AHP (with BAPTA, n = 38; without BAPTA, n = 26). (E) uIPSC recordings from an FSN and a PN, which were recorded by patch electrode solution without and with BAPTA, respectively. (F) uIPSCs in control condition and during 100 nM orexin A application recorded with BAPTA. Note the little effect of orexin A on uIPSCs. (G) Summary of the effects of orexin A on the amplitude, paired-pulse ratio, and failure rate of uIPSCs, where postsynaptic PNs were recorded with the patch electrode solution including BAPTA (n = 10). **P < 0.01, Student's *t*-test.

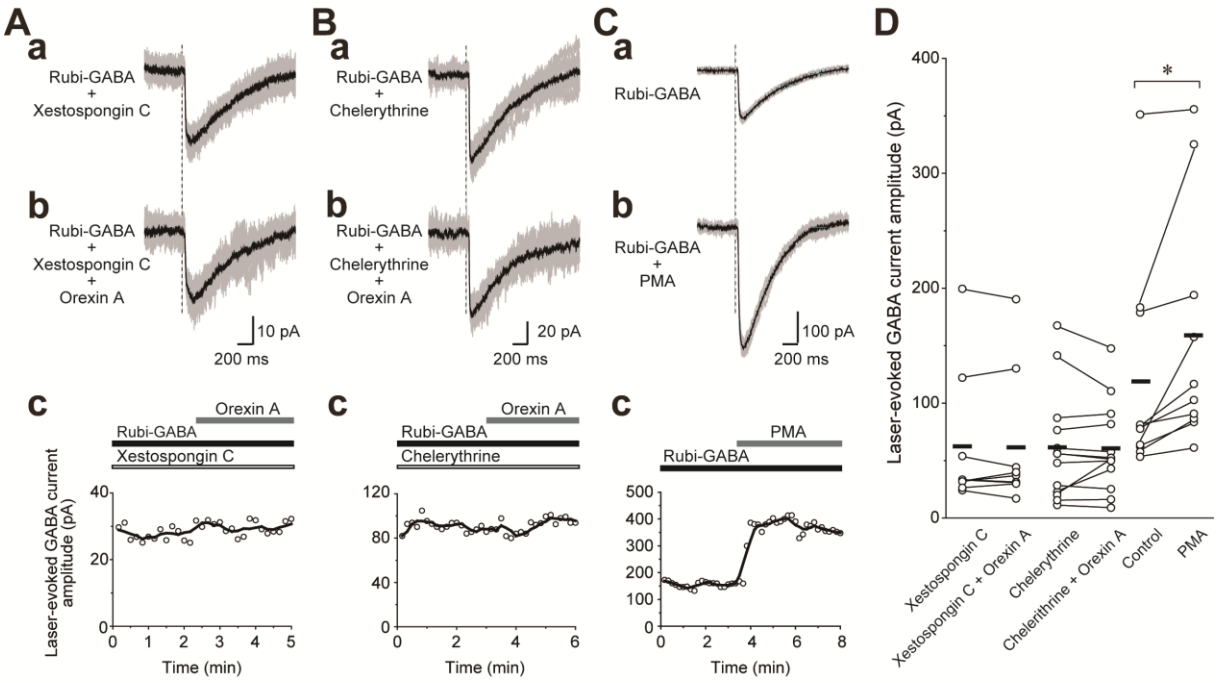

Fig. 14. PKC signalling cascade modulators regulate GABA-mediated currents induced by laser photolysis of Rubi-GABA recorded from PNs. (A) Representative laserevoked GABA-mediated currents (a). Ten consecutive traces (gray) and their average traces (black) are superimposed. The vertical dotted line indicates the timing of photolysis with 473 nm laser. Tetrodotoxin (1 μM), D-AP5 (25 μM), and DNQX (40 μM) were applied in the perfusate. Note that orexin A (100 nM) had little effect on GABA-mediated currents under application of xestospongin C (b). Time course of the GABA-mediated current amplitude was shown in (c). (B) Orexin A had little effect on GABA-mediated currents under application of 1 μM chelerythrine. (C) Phorbol 12-myristate 13-acetate (PMA; 2 μM) enhanced GABA-mediated currents. (D) Summary of the effect of orexin A under application of xestospongin C (n = 9) or chelerythrine (n = 13) and that of PMA (n = 10) on GABA-mediated currents. Horizontal bars indicate the mean. *P < 0.05, paired *t*-test.

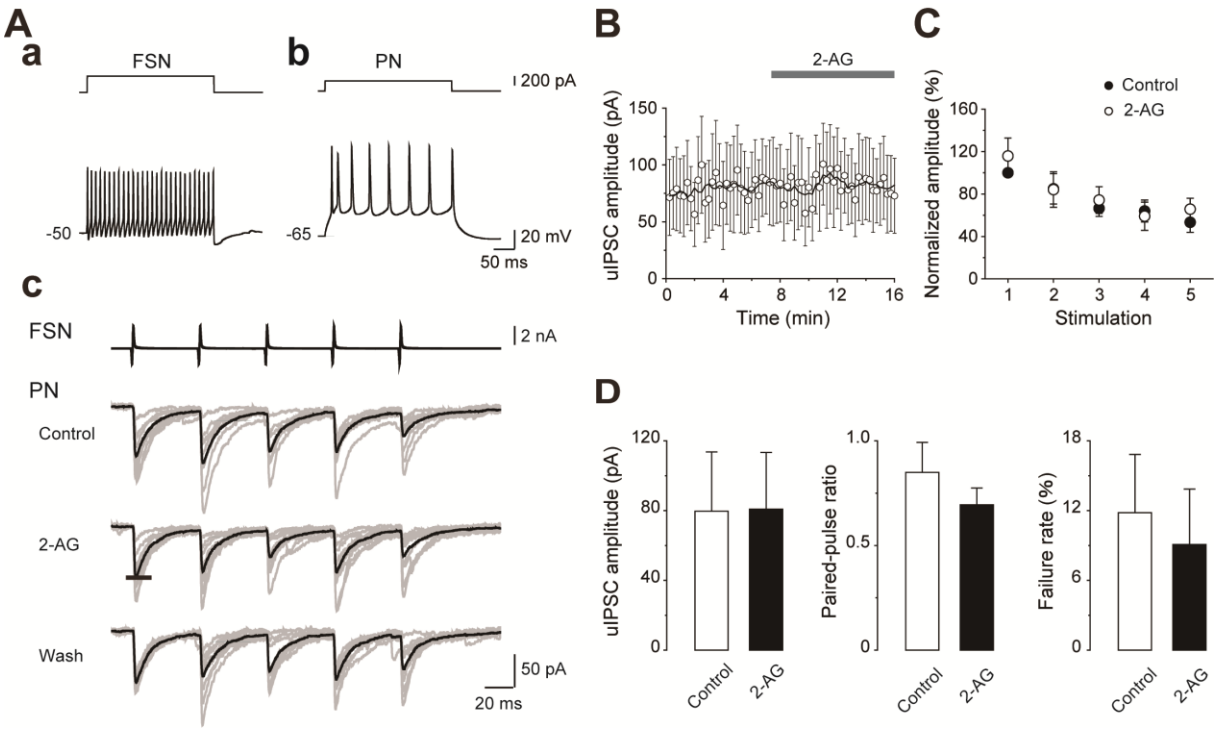

Fig.15 Little effect of 1 μM 2-AG, a selective eCB activator, on uIPSCs in FSN→PN connections. (A) Repetitive spike firing patterns of an FSN (a) and a PN (b), and uIPSCs obtained from an FSN→PN connection before (control), during, and after (wash) bath application of 2-AG (c). Note the little effect of 2-AG on uIPSCs. (B) Time course of the uIPSC amplitude before, during, and after 1 μM 2-AG application in the FSN→PN connections. (C) The normalized amplitude of the 1st to 5th uIPSCs in control and during 2-AG application. (D) Summary of the effects of 2-AG on uIPSC amplitude, paired-pulse ratio, and failure rate in FSN→PN connections (n = 11).